Determination of the $D^0 \to K^+\pi^-$ relative strong phase using quantum-correlated measurements in $e^+e^- \to D^0\bar{D}^0$ at CLEO

D. M. Asner,[1] K. W. Edwards,[1] P. Naik,[1] R. A. Briere,[2] T. Ferguson,[2] G. Tatishvili,[2] H. Vogel,[2] M. E. Watkins,[2] J. L. Rosner,[3] J. P. Alexander,[4] D. G. Cassel,[4] J. E. Duboscq,[4] R. Ehrlich,[4] L. Fields,[4] L. Gibbons,[4] R. Gray,[4] S. W. Gray,[4] D. L. Hartill,[4] B. K. Heltsley,[4] D. Hertz,[4] C. D. Jones,[4] J. Kandaswamy,[4] D. L. Kreinick,[4] V. E. Kuznetsov,[4] H. Mahlke-Krüger,[4] D. Mohapatra,[4] P. U. E. Onyisi,[4] J. R. Patterson,[4] D. Peterson,[4] D. Riley,[4] A. Ryd,[4] A. J. Sadoff,[4] X. Shi,[4] S. Stroiney,[4] W. M. Sun,[4] T. Wilksen,[4] S. B. Athar,[5] R. Patel,[5] J. Yelton,[5] P. Rubin,[6] B. I. Eisenstein,[7] I. Karliner,[7] S. Mehrabyan,[7] N. Lowrey,[7] M. Selen,[7] E. J. White,[7] J. Wiss,[7] R. E. Mitchell,[8] M. R. Shepherd,[8] D. Besson,[9] T. K. Pedlar,[10] D. Cronin-Hennessy,[11] K. Y. Gao,[11] J. Hietala,[11] Y. Kubota,[11] T. Klein,[11] B. W. Lang,[11] R. Poling,[11] A. W. Scott,[11] P. Zweber,[11] S. Dobbs,[12] Z. Metreveli,[12] K. K. Seth,[12] A. Tomaradze,[12] J. Libby,[13] A. Powell,[13] G. Wilkinson,[13] K. M. Ecklund,[14] W. Love,[15] V. Savinov,[15] A. Lopez,[16] H. Mendez,[16] J. Ramirez,[16] J. Y. Ge,[17] D. H. Miller,[17] B. Sanghi,[17] I. P. J. Shipsey,[17] B. Xin,[17] G. S. Adams,[18] M. Anderson,[18] J. P. Cummings,[18] I. Danko,[18] D. Hu,[18] B. Moziak,[18] J. Napolitano,[18] Q. He,[19] J. Insler,[19] H. Muramatsu,[19] C. S. Park,[19] E. H. Thorndike,[19] F. Yang,[19] M. Artuso,[20] S. Blusk,[20] S. Khalil,[20] J. Li,[20] R. Mountain,[20] S. Nisar,[20] K. Randrianarivony,[20] N. Sultana,[20] T. Skwarnicki,[20] S. Stone,[20] J. C. Wang,[20] L. M. Zhang,[20] G. Bonvicini,[21] D. Cinabro,[21] M. Dubrovin,[21] A. Lincoln,[21] and J. Rademacker[22]

(CLEO Collaboration)

[1]*Carleton University, Ottawa, Ontario, Canada K1S 5B6*
[2]*Carnegie Mellon University, Pittsburgh, Pennsylvania 15213, USA*
[3]*Enrico Fermi Institute, University of Chicago, Chicago, Illinois 60637, USA*
[4]*Cornell University, Ithaca, New York 14853, USA*
[5]*University of Florida, Gainesville, Florida 32611, USA*
[6]*George Mason University, Fairfax, Virginia 22030, USA*
[7]*University of Illinois, Urbana-Champaign, Illinois 61801, USA*
[8]*Indiana University, Bloomington, Indiana 47405, USA*
[9]*University of Kansas, Lawrence, Kansas 66045, USA*
[10]*Luther College, Decorah, Iowa 52101, USA*
[11]*University of Minnesota, Minneapolis, Minnesota 55455, USA*
[12]*Northwestern University, Evanston, Illinois 60208, USA*
[13]*University of Oxford, Oxford OX1 3RH, United Kingdom*
[14]*State University of New York at Buffalo, Buffalo, New York 14260, U SA*
[15]*University of Pittsburgh, Pittsburgh, Pennsylvania 15260, USA*
[16]*University of Puerto Rico, Mayaguez, Puerto Rico 00681*
[17]*Purdue University, West Lafayette, Indiana 47907, USA*
[18]*Rensselaer Polytechnic Institute, Troy, New York 12180, USA*
[19]*University of Rochester, Rochester, New York 14627, USA*
[20]*Syracuse University, Syracuse, New York 13244, USA*
[21]*Wayne State University, Detroit, Michigan 48202, USA*
[22]*University of Bristol, Bristol BS8 1TL, United Kingdom*

(Received 18 February 2008; published 30 July 2008)

We exploit the quantum coherence between pair-produced D^0 and $\bar{D}^0$ in $\psi(3770)$ decays to study charm mixing, which is characterized by the parameters x and y, and to make a first determination of the relative strong phase δ between doubly Cabibbo-suppressed $D^0 \to K^+\pi^-$ and Cabibbo-favored $\bar{D}^0 \to K^+\pi^-$. We analyze a sample of 1.0×10^6 $D^0\bar{D}^0$ pairs from 281 pb^{-1} of e^+e^- collision data collected with the CLEO-c detector at $E_{\rm cm} = 3.77$ GeV. By combining CLEO-c measurements with branching fraction input and time-integrated measurements of $R_{\rm M} \equiv (x^2 + y^2)/2$ and $R_{\rm WS} \equiv \Gamma(D^0 \to K^+\pi^-)/\Gamma(\bar{D}^0 \to K^+\pi^-)$ from other experiments, we find $\cos\delta = 1.03^{+0.31}_{-0.17} \pm 0.06$, where the uncertainties are statistical and systematic, respectively. In addition, by further including external measurements of charm mixing parameters, we obtain an alternate measurement of $\cos\delta = 1.10 \pm 0.35 \pm 0.07$, as well as $x\sin\delta = (4.4^{+2.7}_{-1.8} \pm 2.9) \times 10^{-3}$ and $\delta = (22^{+11+9}_{-12-11})^\circ$.

DOI: 10.1103/PhysRevD.78.012001 PACS numbers: 12.15.Ff, 13.20.Fc, 13.25.Ft, 14.40.Lb

I. INTRODUCTION

In the standard model, D^0-$\bar{D}^0$ mixing is suppressed both by the Glashow-Iliopoulos-Maiani mechanism [1] and by Cabibbo-Kobayashi-Maskawa matrix elements [2], although sizeable mixing could arise from new physics [3]. Charm mixing is conventionally described by two small dimensionless parameters:

$$x = 2\frac{M_2 - M_1}{\Gamma_2 + \Gamma_1}, \tag{1}$$

$$y = \frac{\Gamma_2 - \Gamma_1}{\Gamma_2 + \Gamma_1}, \tag{2}$$

where $M_{1,2}$ and $\Gamma_{1,2}$ are the masses and widths, respectively, of the neutral D meson CP eigenstates, D_1 (CP-odd) and D_2 (CP-even), which are defined as follows:

$$|D_1\rangle \equiv \frac{|D^0\rangle + |\bar{D}^0\rangle}{\sqrt{2}}, \tag{3}$$

$$|D_2\rangle \equiv \frac{|D^0\rangle - |\bar{D}^0\rangle}{\sqrt{2}}, \tag{4}$$

assuming CP conservation. The mixing probability is then denoted by $R_M \equiv (x^2 + y^2)/2$, and the width of the D^0 and $\bar{D}^0$ flavor eigenstates is $\Gamma \equiv (\Gamma_1 + \Gamma_2)/2$.

By focusing on D^0 decay times, recent experiments have made precise measurements of D^0-$\bar{D}^0$ mixing parameters [4–8] that highlight the need for information on the relative phase between the Cabibbo-favored decay $D^0 \to K^-\pi^+$ and the doubly Cabibbo-suppressed (DCS) decay $\bar{D}^0 \to K^-\pi^+$. Direct measurements of y come from comparing decay times in $D^0 \to K^-\pi^+$ to those in D^0 transitions to the CP-even eigenstates K^+K^- and $\pi^+\pi^-$. Time-dependent studies of the resonant substructure in $D^0 \to K^0_S\pi^+\pi^-$ provide x as well as y. In contrast, an indirect measure of y is provided by the "wrong-sign" process $D^0 \to K^+\pi^-$, where interference between the DCS amplitude and the mixing amplitude manifests itself in the D^0 decay time distributions. These analyses are sensitive to $y' \equiv y\cos\delta - x\sin\delta$, where $-\delta$ is the relative phase between the DCS amplitude and the corresponding Cabibbo-favored $\bar{D}^0 \to K^+\pi^-$ amplitude: $\langle K^+\pi^-|D^0\rangle / \langle K^+\pi^-|\bar{D}^0\rangle \equiv re^{-i\delta}$. We adopt a convention in which δ corresponds to a strong phase, which vanishes in the SU(3) limit [9]. The magnitude r of the amplitude ratio is approximately 0.06.

Measurements of y and y' have both attained a precision of $\mathcal{O}(10^{-3})$. However, because δ has not previously been measured, these separate determinations of y and y' have not been directly comparable. Thus, even a modest measurement of δ can significantly improve the overall knowledge of charm mixing parameters.

In this article, we present a first determination of δ that takes advantage of the correlated production of D^0 and $\bar{D}^0$ mesons in e^+e^- collisions produced at the Cornell Electron Storage Ring and collected with the CLEO-c detector. If a collision produces no accompanying particles, the $D^0\bar{D}^0$ pair is in a quantum-coherent $C = -1$ state. Because the initial state (the virtual photon) has $J^{PC} = 1^{--}$, there follows a set of selection rules for the decays of the D^0 and $\bar{D}^0$ [3,9–18]. For example, both D^0 and $\bar{D}^0$ cannot decay to CP eigenstates with the same eigenvalue. On the other hand, decays to CP eigenstates of opposite eigenvalue are enhanced by a factor of 2. More generally, final states that can be reached by both D^0 and $\bar{D}^0$ (such as $K^-\pi^+$) are subject to similar interference effects. As a result, the effective D^0 branching fractions in this $D^0\bar{D}^0$ system differ from those measured in isolated D^0 mesons. Moreover, using time-independent rate measurements, it becomes possible to probe D^0-$\bar{D}^0$ mixing as well as the relative strong phases between D^0 and $\bar{D}^0$ decay amplitudes to any given final state.

We implement the method described in Ref. [19] for measuring y and δ using quantum correlations at the $\psi(3770)$ resonance. Our experimental technique is an extension of the double tagging method previously used to determine absolute hadronic D-meson branching fractions at CLEO-c [20]. This method combines yields of fully reconstructed single tags (ST), which are individually reconstructed D^0 or $\bar{D}^0$ candidates, with yields of double tags (DT), which are events where both D^0 and $\bar{D}^0$ are reconstructed, to give absolute branching fractions without needing to know the luminosity or $D^0\bar{D}^0$ production cross section. Given a set of measured yields, efficiencies, and background estimates, a least-squares fitter [21] extracts the number of $D^0\bar{D}^0$ pairs produced ($\mathcal{N}$) and the branching fractions ($\mathcal{B}$) of the reconstructed D^0 final states, while accounting for all statistical and systematic uncertainties and their correlations. We employ a modified version of this fitter that also determines y, x^2, r^2, $r\cos\delta$, and $rx\sin\delta$ using the following categories of reconstructed final states: $K^-\pi^+$ (f), $K^+\pi^-$ ($\bar{f}$), CP-even (S_+) and CP-odd (S_-) eigenstates, and semileptonic decays ($e^\pm$). With CLEO-c measurements alone, r^2 is not determined with sufficient precision to extract δ. Therefore, we also incorporate measurements of branching fractions and mixing parameters from other CLEO-c analyses or from external sources. We neglect CP violation in D decays, which would entail a slight correction to the mixing signal.

The paper is organized as follows. In Sec. II, we review the formalism of quantum-correlated $D^0\bar{D}^0$ decay. Section III describes the event selection criteria and D reconstruction procedures. The external measurements used in the fit are summarized in Sec. IV. Systematic uncertainties, which are also input to the fit, are discussed in Sec. V. Finally, we present and discuss our main fit results in Sec. VI. In the appendix, we provide information for use by other experiments.

II. FORMALISM

To first order in x and y, the C-odd rate $\Gamma_{D^0\bar{D}^0}(i,j)$ for $D^0\bar{D}^0$ decay to final state $\{i,j\}$ follows from the antisymmetric amplitude $\mathcal{M}_{ij}$:

$$\Gamma_{D^0\bar{D}^0}(i,j) \propto \mathcal{M}_{ij}^2 = |A_i\bar{A}_j - \bar{A}_iA_j|^2 = |\langle i|D_2\rangle\langle j|D_1\rangle - \langle i|D_1\rangle\langle j|D_2\rangle|^2, \quad (5)$$

where $A_i \equiv \langle i|D^0\rangle$ and $\bar{A}_i \equiv \langle i|\bar{D}^0\rangle$. These amplitudes are normalized such that $\mathcal{B}_{K^-\pi^+} \approx A^2_{K^-\pi^+}(1 + ry\cos\delta + rx\sin\delta)$, $\mathcal{B}_{S_\pm} \approx A^2_{S_\pm}(1 \mp y)$, and $\mathcal{B}_e \approx A^2_e$. The total rate, $\Gamma_{D^0\bar{D}^0}$, is the same as for uncorrelated decay, as are ST rates. However, unlike the case of uncorrelated $D^0\bar{D}^0$, we can consider the C-odd $D^0\bar{D}^0$ system as a D_1D_2 pair. If only flavored final states are considered, as in Ref. [20], then the effects of quantum correlations are negligible. In this analysis, we also include CP eigenstates, which brings additional sensitivity to y and δ, as demonstrated below.

Quantum-correlated semileptonic rates probe y because the decay width does not depend on the CP eigenvalue of the parent D meson, as this weak decay is only sensitive to flavor content. However, the total width of the parent meson does depend on its CP eigenvalue: $\Gamma_{_1} = \Gamma(1 \mp y)$, so the semileptonic branching fraction for D_1 or D_2 is modified by $1 \pm y$. If we reconstruct a semileptonic decay in the same event as a $D_2 \to S_+$ decay, then the semileptonic D must be a D_1. Therefore, the effective quantum-correlated $D^0\bar{D}^0$ branching fractions ($\mathcal{F}^{\rm cor}$) for $\{S_\pm, e\}$ final states depend on y:

$$\mathcal{F}^{\rm cor}_{S_\pm,e} \approx 2\mathcal{B}_{S_\pm}\mathcal{B}_e(1 \pm y), \quad (6)$$

where the factor of 2 arises from the sum of e^+ and e^- rates. Combined with estimates of $\mathcal{B}_e$ and $\mathcal{B}_{S_\pm}$ from ST yields, external sources, and flavor-tagged semileptonic yields, this equation allows y to be determined.

Similarly, if we reconstruct a $D \to K^-\pi^+$ decay in the same event as a $D_2 \to S_+$, then the $K^-\pi^+$ was produced from a D_1. The effective branching fraction for this DT process is therefore

$$\begin{aligned}\mathcal{F}^{\rm cor}_{S_+,K^-\pi^+} &= |\langle S_+|D_2\rangle\langle K^-\pi^+|D_1\rangle|^2 \\ &\approx \mathcal{B}_{S_+}(1+y)|A_{K^-\pi^+} + \bar{A}_{K^-\pi^+}|^2 \\ &\approx \mathcal{B}_{S_+}\mathcal{B}_{K^-\pi^+}(1+y)(1 - ry\cos\delta - rx\sin\delta) \\ &\quad \times |1 + re^{-i\delta}|^2 \\ &= \mathcal{B}_{S_+}\mathcal{B}_{K^-\pi^+}(1+y)(1 - ry\cos\delta - rx\sin\delta) \\ &\quad \times (1 + 2r\cos\delta + r^2) \\ &\approx \mathcal{B}_{S_+}\mathcal{B}_{K^-\pi^+}(1 + 2r\cos\delta + R_{\rm WS} + y), \end{aligned} \quad (7)$$

where $R_{\rm WS}$ is the wrong-sign rate ratio, which depends on x and y because of the interference between DCS and mixing transitions: $R_{\rm WS} \equiv \Gamma(\bar{D}^0 \to K^-\pi^+)/\Gamma(D^0 \to K^-\pi^+) = r^2 + ry' + R_{\rm M}$. In an analogous fashion, we find $\mathcal{F}^{\rm cor}_{S_-,K^-\pi^+} \approx \mathcal{B}_{S_-}\mathcal{B}_{K^-\pi^+}(1 + R_{\rm WS} - 2r\cos\delta - y)$. When combined with knowledge of $\mathcal{B}_{S_+}$, y, and r, the asymmetry between these two DT yields gives $\cos\delta$. In the absence of quantum correlations, the effective branching fractions above would be $\mathcal{B}_{S_\pm}\mathcal{B}_{K^-\pi^+}(1 + R_{\rm WS})$.

More concretely, we evaluate Eq. (5) with the above definitions of r and δ to produce the expressions in Table I. In doing so, we use the fact that inclusive ST rates are given by the incoherent branching fractions since each event contains one D^0 and one $\bar{D}^0$. Comparison of $\mathcal{F}^{\rm cor}$ with the uncorrelated effective branching fractions, $\mathcal{F}^{\rm unc}$, also given in Table I, allows us to extract r^2, $r\cos\delta$, y, x^2, and

TABLE I. Correlated (C-odd) and uncorrelated effective $D^0\bar{D}^0$ branching fractions, $\mathcal{F}^{\rm cor}$ and $\mathcal{F}^{\rm unc}$, to leading order in x, y, and $R_{\rm WS}$, divided by $\mathcal{B}_i$ for ST modes i (first section) and $\mathcal{B}_i\mathcal{B}_j$ for DT modes $\{i,j\}$ (second section). Charge conjugate modes are implied.

Mode	Correlated	Uncorrelated
$K^-\pi^+$	$1 + R_{\rm WS}$	$1 + R_{\rm WS}$
S_+	2	2
S_-	2	2
$K^-\pi^+$, $K^-\pi^+$	$R_{\rm M}$	$R_{\rm WS}$
$K^-\pi^+$, $K^+\pi^-$	$(1 + R_{\rm WS})^2 - 4r\cos\delta(r\cos\delta + y)$	$1 + R^2_{\rm WS}$
$K^-\pi^+$, S_+	$1 + R_{\rm WS} + 2r\cos\delta + y$	$1 + R_{\rm WS}$
$K^-\pi^+$, S_-	$1 + R_{\rm WS} - 2r\cos\delta - y$	$1 + R_{\rm WS}$
$K^-\pi^+$, e^-	$1 - ry\cos\delta - rx\sin\delta$	1
S_+, S_+	0	1
S_-, S_-	0	1
S_+, S_-	4	2
S_+, e^-	$1 + y$	1
S_-, e^-	$1 - y$	1

$rx\sin\delta$. Information on $\mathcal{B}_i$ is obtained from ST yields at the $\psi(3770)$ and from external measurements using incoherently produced D^0 mesons. These two estimates of $\mathcal{B}_i$ are averaged by the fitter to obtain $\mathcal{F}^{\rm unc}$.

Using only ST and DT yields at the $\psi(3770)$, we can determine y and $\cos\delta$ from the following double ratios, obtained by manipulating the expressions in Table I:

$$y \approx \frac{N_{fe}}{4N_f}\left[\frac{N_{S_-}}{N_{S_-e}} - \frac{N_{S_+}}{N_{S_+e}}\right] \tag{8}$$

$$\approx \frac{1}{4}\left[\frac{N_{S_+e}N_{S_-}}{N_{S_-e}N_{S_+}} - \frac{N_{S_-e}N_{S_+}}{N_{S_+e}N_{S_-}}\right], \tag{9}$$

$$2r\cos\delta + y \approx \frac{N_{f\bar{f}}}{4N_{\bar{f}}}\left[\frac{N_{S_-}}{N_{S_-f}} - \frac{N_{S_+}}{N_{S_+f}}\right] \tag{10}$$

$$\approx \frac{1}{4}N_f N_{S_+S_-}\left[\frac{1}{N_{fS_-}N_{S_+}} - \frac{1}{N_{fS_+}N_{S_-}}\right], \tag{11}$$

where N denotes an efficiency-corrected background-subtracted ST or DT yield. Note that semileptonic yields are essential for separating y and $\cos\delta$. Including external branching fractions provides additional ways to determine y and $\cos\delta$:

$$y = \pm\left[1 - \frac{2\mathcal{N}\mathcal{B}_{S_\pm}\mathcal{B}_e}{N_{S_\pm e}}\right], \tag{12}$$

$$2r\cos\delta + y = (1 + R_{\rm WS})\left[\frac{N_{S_+f}/\mathcal{B}_{S_+} - N_{S_-f}/\mathcal{B}_{S_-}}{N_{S_+f}/\mathcal{B}_{S_+} + N_{S_-f}/\mathcal{B}_{S_-}}\right]. \tag{13}$$

Although we neglect x^2 and y^2 terms in general, we report a result for x^2 as determined solely from $N_{ff}/N_{f\bar{f}}$.

III. EVENT SELECTION AND RECONSTRUCTION

Our current analysis uses 281 pb^{-1} of $e^+e^- \to \psi(3770)$ data collected with the CLEO-c [22–26] detector. We also make use of a large Monte Carlo simulated sample of uncorrelated $D^0\bar{D}^0$ decays with an effective luminosity 40 times that of our data sample, from which we estimate signal efficiencies, background contributions, and probabilities for misreconstructing a produced signal decay in a different signal mode (cross feed). In these samples, we reconstruct the final states shown in Table II, with $\pi^0 \to \gamma\gamma$, $\eta \to \gamma\gamma$, $K^0_S \to \pi^+\pi^-$, and $\omega \to \pi^+\pi^-\pi^0$. Because most K^0_L mesons and neutrinos are not detected, we do not reconstruct $K^0_L\pi^0$ and semileptonic ST modes; they are only included in DT modes, paired with a fully reconstructed D candidate. Below, we denote by S'_+ the subset of S_+ modes that are fully reconstructed: K^+K^-, $\pi^+\pi^-$, and $K^0_S\pi^0\pi^0$. For CP eigenstates, we choose modes with unambiguous CP content. In addition to two-body decays, we also include $K^0_S\pi^0\pi^0$, which is a pure CP-even eigenstate because the two identical π^0's must have even angular momentum in order to satisfy Bose symmetry. We neglect CP violation in K^0 decays.

TABLE II. D final states reconstructed in this analysis.

Type	Final states
Flavored	$K^-\pi^+$, $K^+\pi^-$
S_+	K^+K^-, $\pi^+\pi^-$, $K^0_S\pi^0\pi^0$, $K^0_L\pi^0$
S_-	$K^0_S\pi^0$, $K^0_S\eta$, $K^0_S\omega$
$e^\pm$	Inclusive $Xe^+\nu_e$, $Xe^-\bar{\nu}_e$

Standard CLEO-c selection criteria for $\pi^\pm$, $K^\pm$, π^0, and K^0_S candidates are described in Ref. [27]. In addition, for K^0_S candidates, we impose $|M(\pi^+\pi^-) - M_{K^0_S}| < 7.5\ {\rm MeV}/c^2$, and we require the decay vertex to be separated from the interaction region with a significance greater than 2 standard deviations (σ). For the $K^0_S\pi^0\pi^0$ mode, we reject K^0_S daughter tracks with ionization energy loss consistent with being kaons at the level of 2σ in order to suppress misreconstructed $D \to K^-\pi^+\pi^0$ decays, where the kaon is taken to be a charged pion, and a soft combinatoric π^0 candidate is incorporated into the D candidate. We accept ω candidates with $|M(\pi^+\pi^-\pi^0) - M_\omega| < 20\ {\rm MeV}/c^2$. Reconstruction of $\eta \to \gamma\gamma$ proceeds analogously to $\pi^0 \to \gamma\gamma$. In addition, we require $|M(\gamma\gamma) - M_\eta| < 42\ {\rm MeV}/c^2$. All invariant mass requirements correspond to approximately 3σ consistency with the nominal masses from Ref. [28].

A. Single tags

Reconstruction of all modes in this analysis, including DT modes, begins with fully reconstructed ST D candidates, which are identified using two kinematic variables that express momentum and energy conservation: the beam-constrained candidate mass M and the energy difference ΔE. These variables are defined to be

TABLE III. Requirements on ΔE for D candidates.

Mode	Requirement (GeV)
$K^-\pi^+$	$\lvert\Delta E\rvert < 0.0294$
$K^+\pi^-$	$\lvert\Delta E\rvert < 0.0294$
K^+K^-	$\lvert\Delta E\rvert < 0.0200$
$\pi^+\pi^-$	$\lvert\Delta E\rvert < 0.0300$
$K^0_S\pi^0\pi^0$	$-0.0550 < \Delta E < 0.0450$
$K^0_S\pi^0$	$-0.0710 < \Delta E < 0.0450$
$K^0_S\eta$	$-0.0550 < \Delta E < 0.0350$
$K^0_S\omega$	$\lvert\Delta E\rvert < 0.0250$

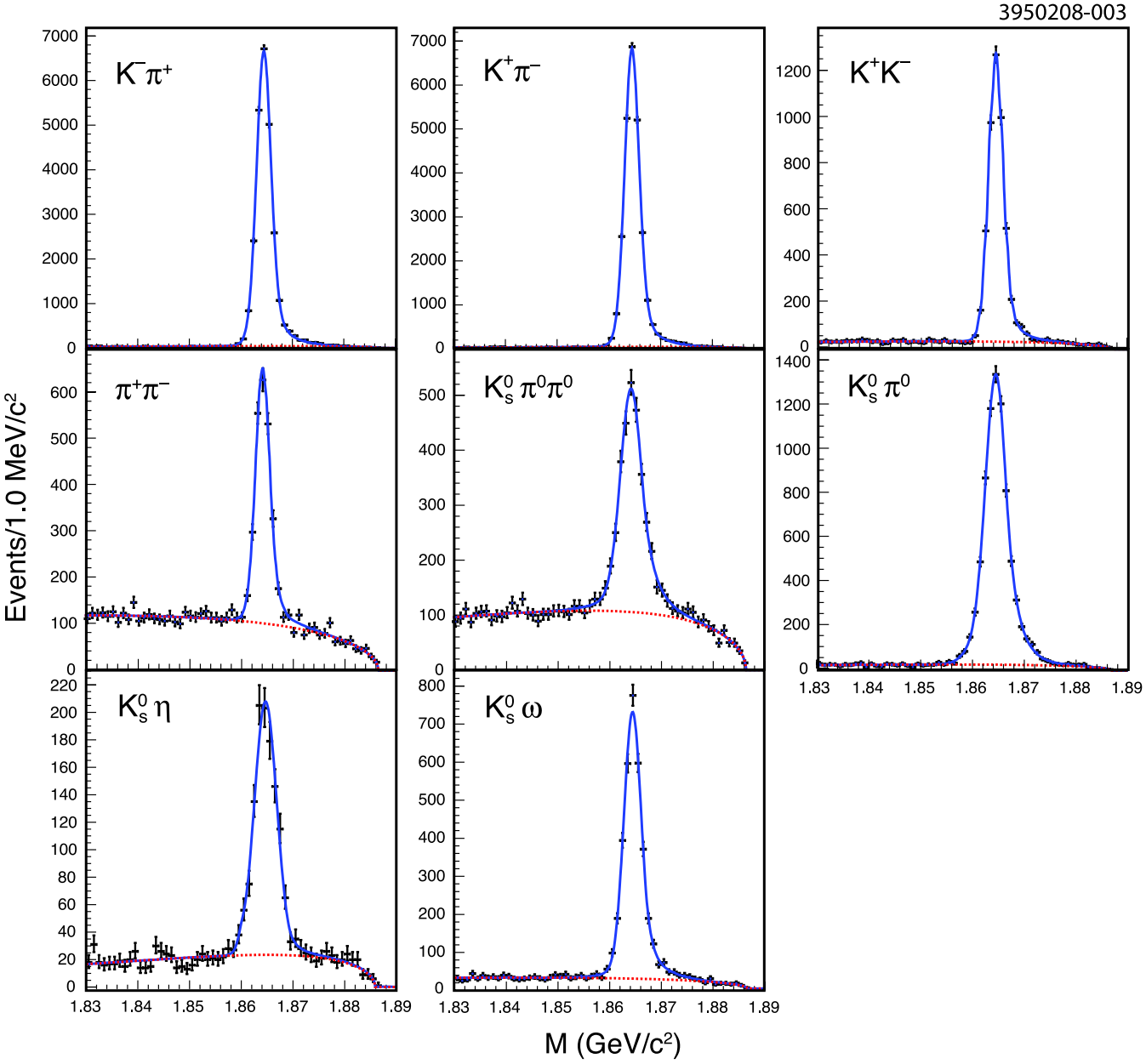

FIG. 1 (color online). ST M distributions and fits. Data are shown as points with error bars. The solid lines show the total fits and the dashed lines show the background shapes.

$$M \equiv \sqrt{E_0^2/c^4 - \mathbf{p}_D^2/c^2}, \tag{14}$$

$$\Delta E \equiv E_D - E_0, \tag{15}$$

where $\mathbf{p}_D$ and E_D are the total momentum and energy of the D candidate, and E_0 is the beam energy. Correctly reconstructed D candidates produce a peak in M at the D mass and in ΔE at zero. We determine ST yields by fitting the M distribution with the mode-dependent requirements on ΔE listed in Table III, which are applied to both ST and DT D candidates. The limits are set at approximately 3 standard deviations. Modes with π^0 or η, which decay to

TABLE IV. ST yields and efficiencies input to the data fit. Yield uncertainties are statistical and uncorrelated systematic, respectively, and efficiency uncertainties are statistical only.

Mode	Yield	Efficiency (%)
$K^-\pi^+$	25374 ± 166 ± 26	64.70 ± 0.04
$K^+\pi^-$	25842 ± 167 ± 26	65.62 ± 0.04
K^+K^-	4740 ± 71 ± 5	57.25 ± 0.09
$\pi^+\pi^-$	2098 ± 59 ± 9	72.92 ± 0.13
$K^0_S\pi^0\pi^0$	2435 ± 72 ± 16	12.50 ± 0.06
$K^0_S\pi^0$	7523 ± 91 ± 17	29.73 ± 0.05
$K^0_S\eta$	1051 ± 39 ± 17	10.34 ± 0.06
$K^0_S\omega$	3239 ± 63 ± 7	12.48 ± 0.04

two photons, have asymmetric limits to allow for partially contained showers in the electromagnetic calorimeter.

For $K^{\pm}\pi^{\mp}$, K^+K^-, and $\pi^+\pi^-$ ST modes, in events containing only two tracks, we suppress cosmic muons and Bhabhas scattering events by vetoing tracks that are identified as muons or electrons and by requiring at least one electromagnetic shower in the calorimeter above 50 MeV not associated with the signal tracks. For K^+K^- ST candidates, additional geometric requirements are needed to remove doubly radiative Bhabhas followed by pair conversion of a radiated photon. Also, we accept only one candidate per mode per event; when multiple candidates are present, we choose the one with smallest $|\Delta E|$.

The resultant M distributions, shown in Fig. 1, are fitted to a signal shape derived from simulated signal events and to a background ARGUS function [29]. The simulated signal shape is both shifted and convoluted with a Gaussian smearing function to account for imperfect modeling of the detector resolution and beam energy calibration. The width of the smearing function is allowed to float in the fit. The measured ST yields and efficiencies are given in Table IV. The yield uncertainties are statistical and uncorrelated systematic, respectively. The latter arise from modeling of multiple candidates in simulation and variations in the signal line shape. Correlated systematic uncertainties are discussed separately in Sec. V.

B. Fully reconstructed hadronic double tags

Except for modes with $K^0_L\pi^0$, we form hadronic DTs by combining two ST candidates passing the above selection criteria. Multiple candidates are resolved after forming the DT candidates, not at the ST level. We choose one candidate per mode per event with $\bar{M}$ closest to the measured D^0 mass, where $\bar{M} \equiv [M(D^0) + M(\bar{D}^0)]/2$. We extract signal yields by counting events in the two-dimensional $M(D^0)$ vs $M(\bar{D}^0)$ plane, as illustrated in Fig. 2. The signal region S is defined to be approximately 3 standard deviations in each dimension: $1.86 < M(D^0) < 1.87$ GeV/c^2 and $1.86 <$

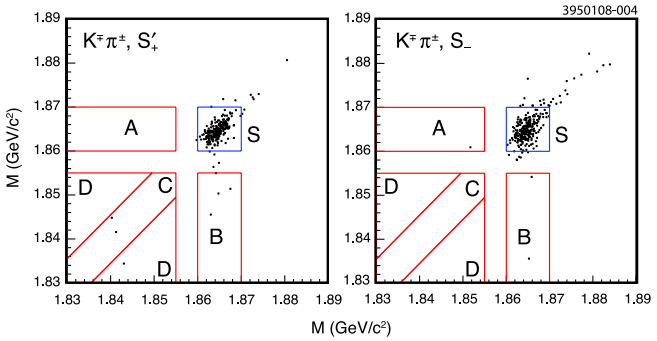

FIG. 2 (color online). Two-dimensional M distributions with signal (S) and sideband (A, B, C, D) regions depicted, for the sum of all $\{K^{\mp}\pi^{\pm}, S'_+\}$ and $\{K^{\mp}\pi^{\pm}, S_-\}$ modes listed in Table V.

TABLE V. Fully reconstructed DT yields and efficiencies input to the data fit. Yield uncertainties are statistical and uncorrelated systematic (for sideband subtraction), respectively, and efficiency uncertainties are statistical only.

Mode	Yield	Efficiency (%)
$K^-\pi^+$, $K^-\pi^+$	$2.0 \pm 1.4 \pm 0$	36.1 ± 3.4
$K^-\pi^+$, $K^+\pi^-$	$600 \pm 25 \pm 5$	41.1 ± 0.2
$K^-\pi^+$, K^+K^-	$71 \pm 8 \pm 1$	35.5 ± 0.6
$K^-\pi^+$, $\pi^+\pi^-$	$24 \pm 5 \pm 1$	44.4 ± 1.1
$K^-\pi^+$, $K^0_S\pi^0\pi^0$	$32 \pm 6 \pm 1$	8.0 ± 0.3
$K^-\pi^+$, $K^0_S\pi^0$	$88 \pm 9 \pm 1$	18.4 ± 0.3
$K^-\pi^+$, $K^0_S\eta$	$8.0 \pm 2.8 \pm 0.0$	6.0 ± 0.3
$K^-\pi^+$, $K^0_S\omega$	$29 \pm 5 \pm 0$	8.7 ± 0.2
$K^+\pi^-$, $K^+\pi^-$	$2.0 \pm 1.4 \pm 0.0$	44.1 ± 3.3
$K^+\pi^-$, K^+K^-	$54 \pm 7 \pm 0$	36.1 ± 0.6
$K^+\pi^-$, $\pi^+\pi^-$	$25 \pm 5 \pm 1$	48.1 ± 1.1
$K^+\pi^-$, $K^0_S\pi^0\pi^0$	$33 \pm 6 \pm 0$	8.0 ± 0.3
$K^+\pi^-$, $K^0_S\pi^0$	$76 \pm 9 \pm 0$	18.6 ± 0.3
$K^+\pi^-$, $K^0_S\eta$	$9 \pm 3 \pm 0$	6.1 ± 0.3
$K^+\pi^-$, $K^0_S\omega$	$33 \pm 6 \pm 1$	8.0 ± 0.2
K^+K^-, $K^0_S\pi^0$	$39 \pm 6 \pm 1$	17.1 ± 0.6
K^+K^-, $K^0_S\eta$	$7.0 \pm 2.7 \pm 0.0$	7.1 ± 0.8
K^+K^-, $K^0_S\omega$	$20 \pm 4 \pm 0$	6.8 ± 0.4
$\pi^+\pi^-$, $K^0_S\pi^0$	$13 \pm 4 \pm 0$	19.2 ± 1.2
$\pi^+\pi^-$, $K^0_S\eta$	$2.0 \pm 1.4 \pm 0.0$	8.1 ± 1.4
$\pi^+\pi^-$, $K^0_S\omega$	$7.0 \pm 2.7 \pm 0.0$	9.9 ± 0.9
$K^0_S\pi^0\pi^0$, $K^0_S\pi^0$	$14 \pm 4 \pm 0$	3.5 ± 0.2
$K^0_S\pi^0\pi^0$, $K^0_S\eta$	$4.0 \pm 2.0 \pm 0.0$	1.2 ± 0.2
$K^0_S\pi^0\pi^0$, $K^0_S\omega$	$4.0 \pm 2.0 \pm 0.0$	1.4 ± 0.2

$M(\bar{D}^0) < 1.87$ GeV/c^2. Sidebands A and B contain candidates where either the D^0 or the $\bar{D}^0$ is misreconstructed. Sidebands C and D contain candidates where both D^0 and $\bar{D}^0$ are misreconstructed, either in a correlated way (C) by assigning daughter particles to the wrong parent or in an uncorrelated way (D). Event counts in sidebands A, B, and C are projected into the signal region S using scale factors determined from integrating the background shape in the ST M fits. Contributions to sideband D are assumed to be uniformly distributed across the other regions. To account for systematic effects in the sideband definitions and in the extrapolation to the signal regions, we assign a 100% systematic uncertainty on the size of the sideband subtractions, which is much smaller than the statistical uncertainties in all cases.

Table V gives the fully reconstructed DT yields and efficiencies input to the fit, and Fig. 3 shows the corresponding $\bar{M}$ projections. Same-CP $\{S_+, S_+\}$ modes are not included in the standard fit.

C. Semileptonic double tags

Semileptonic DTs are partially reconstructed by combining a fully reconstructed hadronic ST with an electron candidate from the remainder of the event. The hadronic

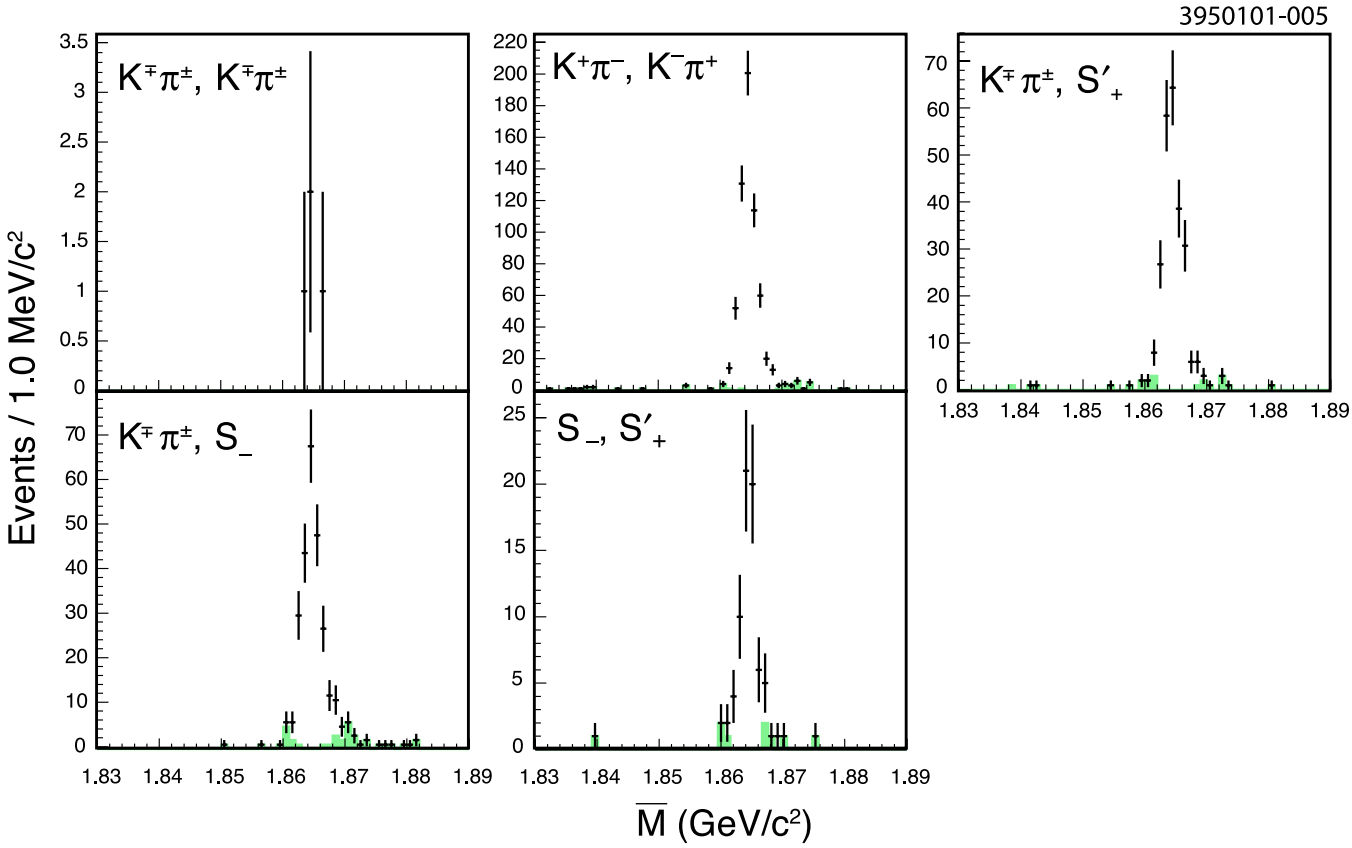

FIG. 3 (color online). Sums of fully reconstructed DT $\bar{M}$ distributions, with charge conjugate modes implied. Data are shown as points with error bars. The shaded histograms show events outside the signal region.

tags are selected using the same criteria as for STs, described in Sec. III A, with an additional mode-dependent M requirement listed in Table VI. The limits are set at approximately 3 standard deviations. Multiple tag candidates are resolved with minimal $|\Delta E|$, as for STs. All electron candidates in a given event are accepted.

Electron candidate tracks are selected using the criteria described in Ref. [30]. Electrons are distinguished from hadrons via a multivariate discriminant that combines information from the ratio of the energy deposited in the calorimeter to the measured track momentum (E/p), ionization energy loss in the tracking chambers (dE/dx), and the ring-imaging Čerenkov counter (RICH). When paired with a $K^{\mp}\pi^{\pm}$ tag, the kaon and electron charges must be the same. This requirement removes charge-symmetric backgrounds and cannot be used with unflavored $S_{\pm}$ tag modes.

TABLE VI. Requirements on M for hadronic tags in semileptonic DT candidates.

Mode	Requirement (GeV/c^2)
$K^-\pi^+$	$1.8585 < M < 1.8775$
$K^+\pi^-$	$1.8585 < M < 1.8775$
K^+K^-	$1.8585 < M < 1.8775$
$\pi^+\pi^-$	$1.8585 < M < 1.8775$
$K^0_S\pi^0\pi^0$	$1.8530 < M < 1.8780$
$K^0_S\pi^0$	$1.8530 < M < 1.8780$
$K^0_S\eta$	$1.8585 < M < 1.8775$
$K^0_S\omega$	$1.8585 < M < 1.8775$

As illustrated in Fig. 4, the resulting electron momentum spectrum for each tag mode is fit to signal and background shapes fixed by the simulation; only the normalizations are allowed to float. We correct the simulated signal spectrum for relative bin-by-bin efficiency differences between data and simulation, which are measured with a high-statistics radiative Bhabha sample. The background components in the spectrum fit include misreconstructed tags, photon conversions and light hadron decays to electrons (mostly π^0 Dalitz decays), weak decays in flight, and hadron misidentification. The latter component peaks at 700 MeV/c and mostly consists of $K^{\pm}$ that escape the acceptance of the RICH; $K^{\pm}$ are indistinguishable from $e^{\pm}$ using dE/dx at this momentum. In the fit, the misreconstructed tag component is fixed from sidebands in M and ΔE. The other backgrounds contribute approximately 7% for $K^{\mp}\pi^{\pm}$ tags and 20%–30% for $S_{\pm}$ tags.

Table VII gives the semileptonic DT yields and efficiencies input to the fit. The uncorrelated systematic uncertain-

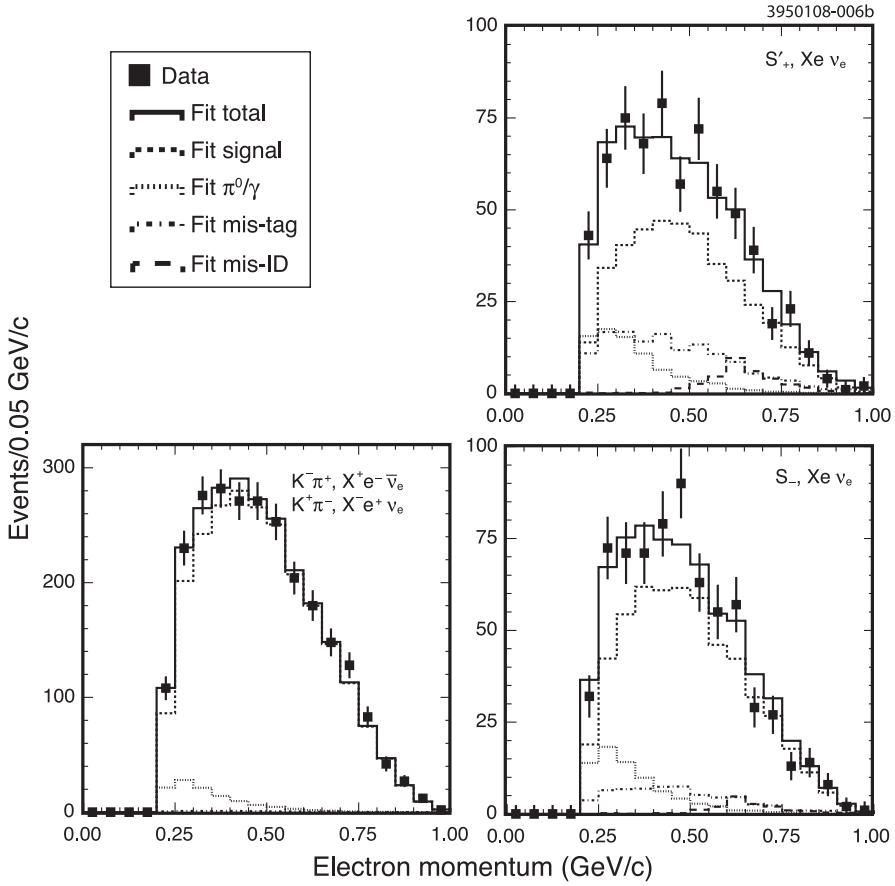

FIG. 4. Sums of electron momentum spectra for $X^- e^+ \nu_e$ and $X^+ e^- \bar{\nu}_e$. Data are shown as points with error bars, and the histograms show the signal and background components in the fits.

ties are determined from yield excursions under variation of the signal and background shapes used in the spectrum fit. For the signal shape, we adjust the semileptonic form factor model used in the simulation. For the background shapes, we vary the allowed background composition by removing components with insignificant yields and also allowing for negative normalizations.

TABLE VII. Semileptonic DT yields and efficiencies input to the data fit. Yield uncertainties are statistical and uncorrelated systematic, respectively, and efficiency uncertainties are statistical only.

Mode	Yield	Efficiency (%)
$X^+ e^- \bar{\nu}_e$, $K^- \pi^+$	$1128 \pm 45 \pm 13$	45.3 ± 0.2
$X^+ e^- \bar{\nu}_e$, $K^- K^+$	$128 \pm 24 \pm 5$	40.1 ± 0.5
$X^+ e^- \bar{\nu}_e$, $\pi^- \pi^+$	$49 \pm 12 \pm 7$	50.3 ± 0.9
$X^+ e^- \bar{\nu}_e$, $K^0_S \pi^0 \pi^0$	$37 \pm 22 \pm 12$	8.9 ± 0.2
$X^+ e^- \bar{\nu}_e$, $K^0_S \pi^0$	$195 \pm 24 \pm 2$	21.4 ± 0.3
$X^+ e^- \bar{\nu}_e$, $K^0_S \eta$	$28 \pm 6 \pm 4$	7.9 ± 0.3
$X^+ e^- \bar{\nu}_e$, $K^0_S \omega$	$50 \pm 15 \pm 6$	8.2 ± 0.2
$X^- e^+ \nu_e$, $K^+ \pi^-$	$1218 \pm 47 \pm 17$	45.9 ± 0.2
$X^- e^+ \nu_e$, $K^- K^+$	$102 \pm 21 \pm 10$	39.0 ± 0.5
$X^- e^+ \nu_e$, $\pi^- \pi^+$	$40 \pm 10 \pm 4$	50.5 ± 0.8
$X^- e^+ \nu_e$, $K^0_S \pi^0 \pi^0$	$50 \pm 15 \pm 9$	9.6 ± 0.2
$X^- e^+ \nu_e$, $K^0_S \pi^0$	$189 \pm 19 \pm 7$	21.4 ± 0.3
$X^- e^+ \nu_e$, $K^0_S \eta$	$27 \pm 8 \pm 2$	7.7 ± 0.3
$X^- e^+ \nu_e$, $K^0_S \omega$	$49 \pm 16 \pm 4$	8.5 ± 0.2

D. Double tags with $K^0_L \pi^0$

DT modes with $K^0_L \pi^0$ are reconstructed with the missing mass technique also used in Ref. [31]. A fully recon-

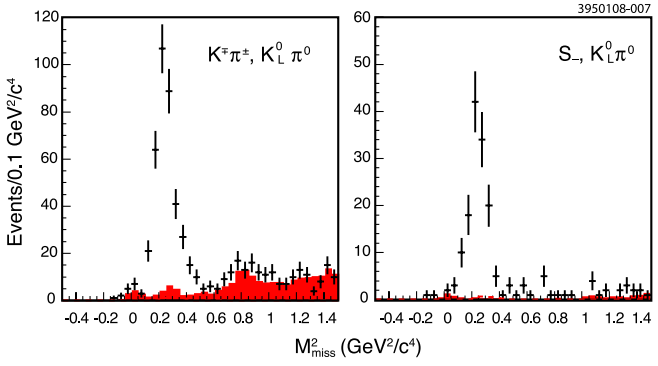

FIG. 5 (color online). Sums of $M^2_{\rm miss}$ distributions for $K^0_L \pi^0$. The shaded histograms represent simulations of the peaking backgrounds $D^0 \to \pi^0 \pi^0$, $K^0_S \pi^0$, $\eta \pi^0$, and $K^{*0} \pi^0$.

TABLE VIII. $K^0_L\pi^0$ DT yields and efficiencies with statistical uncertainties input to the data fit.

Mode	Yield	Efficiency (%)
$K^0_L\pi^0$, $K^-\pi^+$	187 ± 14	34.0 ± 0.2
$K^0_L\pi^0$, $K^+\pi^-$	179 ± 14	34.8 ± 0.2
$K^0_L\pi^0$, $K^0_S\pi^0$	90 ± 10	15.5 ± 0.1
$K^0_L\pi^0$, $K^0_S\eta$	8.6 ± 3.1	5.4 ± 0.1
$K^0_L\pi^0$, $K^0_S\omega$	34 ± 6	6.2 ± 0.1

structed ST candidate, selected as described in Sec. III A, is combined with a π^0 candidate, and we compute the squared recoil mass against the ST-π^0 system, $M^2_{\rm miss}$. Signal $K^0_L\pi^0$ decays produce a peak in $M^2_{\rm miss}$ at $M_{K^0_L}$. Backgrounds from $D \to K^0_S\pi^0$, $\pi^0\pi^0$, and $\eta\pi^0$ are suppressed by vetoing events with additional unassigned charged particles, η, or π^0 candidates.

Figure 5 shows the resultant $M^2_{\rm miss}$ in data. Signal yields are obtained from event counts in the signal region of $0.1 < M^2_{\rm miss} < 0.5$ GeV$^2/c^4$. The contribution from combinatoric background is estimated from the $0.8 < M^2_{\rm miss} < 1.2$ GeV$^2/c^4$ sideband to be $\mathcal{O}(10^{-3})$ and is subtracted. The residual background contributions from $K^0_S\pi^0$ and $\eta\pi^0$, which peak in the signal region, and from $\pi^0\pi^0$, which peaks below the signal region, are estimated from simulated data and are subtracted by the fitter, as described in Sec. III E.

Table VIII lists the $K^0_L\pi^0$ DT yields and efficiencies input to the fit. There are no uncorrelated systematic uncertainties for these modes.

E. Cross feed and peaking backgrounds

The yields in Tables IV, V, VII, and VIII include peaking backgrounds contributions and cross feed among signal modes that are subtracted by the fitter. To do so, the fitter makes use of cross feed probabilities and background efficiencies determined from simulated events, as well as branching fractions for peaking background processes [28]. These inputs are listed in Table IX. The correlated uncertainties among these contributions is also accounted for.

In most cases, the peaking background processes produce the same final state particles as the signal modes to which they contribute. For these backgrounds, the DT contribution is assumed to occur at the same rate as for STs. Other backgrounds, indicated by asterisks in Table IX, arise from misreconstructed D decays. These backgrounds are present only in ST modes and do not contribute to DT modes because of the kinematic constraints of full event reconstruction. Background processes are identified using simulated $D^0\bar{D}^0$ events, where each D is uncorrelated with

TABLE IX. Cross feed probabilities and peaking background efficiencies and branching fractions input to the fit. Backgrounds marked by an asterisk (*) occur only in STs, not DTs.

Cross feed → Signal		Probability (%)
$K^+\pi^- \to K^-\pi^+$		0.098 ± 0.005
$K^-\pi^+ \to K^+\pi^-$		0.092 ± 0.003
$K^0_S\omega \to K^0_S\pi^0\pi^0$		0.048 ± 0.031
$K^0_S\pi^0 \to K^0_L\pi^0$		1.92 ± 0.03
Background → Signal	$\mathcal{B}_{\rm bkg}$ (%) [28]	Efficiency (%)
$K^0_S\pi^+\pi^- \to K^0_S\pi^0\pi^0$	2.90 ± 0.19	0.006 ± 0.012
$\pi^+\pi^-\pi^0\pi^0 \to K^0_S\pi^0\pi^0$	0.98 ± 0.09	0.029 ± 0.067
$K^-\pi^+\pi^0(^*) \to K^0_S\pi^0\pi^0$	14.1 ± 0.5	0.0012 ± 0.0024
$D^+ \to K^0_S\pi^+\pi^0(^*) \to K^0_S\pi^0\pi^0$	7.22 ± 0.26	0.048 ± 0.007
$\rho^+\pi^- \to K^0_S\pi^0$	1.00 ± 0.06	0.071 ± 0.005
$\rho^0\pi^0 \to K^0_S\pi^0$	0.32 ± 0.04	0.032 ± 0.033
Generic $D^0\bar{D}^0(^*) \to K^0_S\pi^0$	...	0.00051 ± 0.00016
Generic $D^+D^-(^*) \to K^0_S\pi^0$	...	0.00038 ± 0.00012
$\bar{K}^{*0}\pi^+\pi^- \to K^0_S\omega$	2.3 ± 0.5	0.065 ± 0.002
$K^{*-}\pi^+\pi^0 \to K^0_S\omega$	1.00 ± 0.22	0.135 ± 0.003
$K^{*-}\rho^+ \to K^0_S\omega$	6.4 ± 2.5	0.035 ± 0.001
$\bar{K}^{*0}\rho^0 \to K^0_S\omega$	1.50 ± 0.33	0.022 ± 0.004
$K^0_S\pi^+\pi^-\pi^0 \to K^0_S\omega$	1.1 ± 1.1	0.405 ± 0.423
$\pi^+\pi^-\pi^+\pi^-\pi^0 \to K^0_S\omega$	0.41 ± 0.05	0.006 ± 0.003
$K^-_1\pi^+ \to K^0_S\omega$	1.12 ± 0.31	0.038 ± 0.005
$\bar{K}^0_1\pi^0 \to K^0_S\omega$	0.59 ± 0.02	0.030 ± 0.010
$\eta\pi^0 \to K^0_L\pi^0$	0.056 ± 0.014	0.155 ± 0.001
$\pi^0\pi^0 \to K^0_L\pi^0$	0.079 ± 0.008	0.117 ± 0.001

TABLE X. External branching ratio measurements and their correlations used in the data fit. An asterisk (*) indicates removal of overlapping CLEO-c measurements.

Parameter	Value (%)	Correlation Coefficients						
$\mathcal{B}(K^-\pi^+)$	3.81 ± 0.09 [32]	1	0.08	0.06	0.04	−0.08	0	0
$\mathcal{B}(K^0_S\pi^0)$	1.15 ± 0.12 [32]		1	0.58	0.14	−0.95	0	0
$\mathcal{B}(K^0_S\eta)$	0.380 ± 0.060 [32]			1	0.10	−0.55	0	0
$\mathcal{B}(K^0_S\omega)$	1.30 ± 0.30 [32]				1	−0.13	0	0
$\mathcal{B}(K^0_L\pi^0)$	1.003 ± 0.083* [31]					1	0	0
$\mathcal{B}(K^-K^+)/\mathcal{B}(K^-\pi^+)$	10.10 ± 0.16 [28]						1	0.30
$\mathcal{B}(\pi^-\pi^+)/\mathcal{B}(K^-\pi^+)$	3.588 ± 0.057* [28]							1

the other and decays generically. Background efficiencies are determined by observing the change in signal yield as each background contribution is removed from the simulated sample.

We also adjust the peaking background estimates for quantum correlation effects. The background branching fractions and efficiencies mentioned above assume uncorrelated D decay, but the background estimate also depends on the type of decay of the other D. For instance, $K^0_L\pi^0$ signals have cross feed background from $K^0_S\pi^0$ but only for $K\pi$ and CP-even tags. In $K^0_L\pi^0$ candidates opposite CP-odd tags, $K^0_S\pi^0$ cannot contribute because it is also CP-odd. For non-CP-eigenstate multibody backgrounds, we assume equal CP-eigenstate and flavored content, with the CP-eigenstate content equally divided between CP-even and CP-odd. Variations in these assumptions give rise to systematic uncertainties, which are assessed in Sec. VI. In general, peaking backgrounds account for less than 1% of the measured yields, except in $K^0_S\omega$ modes (5%–10%), $K^0_L\pi^0$ modes (1%–2%), and ST $K^0_S\pi^0\pi^0$ (3%).

IV. EXTERNAL MEASUREMENTS

As discussed in Sec. II, external estimates of uncorrelated branching fractions can help determine y and δ. We include measurements from Refs. [28,32] and from other CLEO-c analyses along with their full error matrix in the fit. For the CLEO-c analyses, we account for statistical correlations with the yields measured in this analysis. Tables X, XI, and XII show the sources of these measurements, and there is no overlap among the measurements in these tables.

A. External branching ratio measurements

Because our precision on $\cos\delta$ is currently limited by our knowledge of the CP-eigenstate branching fractions, we include as many external measurements of these branching fractions as possible. Except for the inclusive $\mathcal{B}(K^0_S\pi^0\pi^0)$ and $\mathcal{B}(K^0_L\pi^0)$, all CP-eigenstates in this analysis have previous branching ratio measurements with respect to other reference modes.

For $K^0_S\pi^0$, $K^0_S\eta$, and $K^0_S\omega$, we make use of the global branching fraction fit performed in Ref. [32]. Because $\mathcal{B}(K^-\pi^+)$ is a free parameter in this fit and in the current analysis, we also include Ref. [32]'s fit result for this mode in order to properly account for the correlations among these branching fractions. We do not use Ref. [28] because this compilation includes a CLEO-c measurement of $\mathcal{B}(K^-\pi^+)$ [20], which is correlated with the measurements in this analysis.

Previous experiments have measured $R_{KK} \equiv \mathcal{B}(K^-K^+)/\mathcal{B}(K^-\pi^+)$ and $R_{\pi\pi} \equiv \mathcal{B}(\pi^-\pi^+)/\mathcal{B}(K^-\pi^+)$ simultaneously [28], so these two quantities are correlated both statistically [via the common denominator, $\mathcal{B}(K^-\pi^+)$] and systematically. It is common for these experiments to also report a value of $R_{KK}/R_{\pi\pi}$ in addition to R_{KK} and $R_{\pi\pi}$ separately. Using the dominant measurements of all three quantities [40,48–50], we compute a weighted average correlation coefficient of 0.30 between the R_{KK} and $R_{\pi\pi}$ values quoted in Ref. [28]. For $R_{\pi\pi}$, we remove the CLEO-c measurement [51] from the average because it was based on the same data set as this analysis.

The CLEO-c $D \to K^0_{S/L}\pi^0$ analysis [31] provides additional information on $\mathcal{B}(K^0_L\pi^0)$ from the $K^-\pi^+\pi^0$ and $K^-\pi^+\pi^-\pi^+$ tag modes, which are not used in this analysis. Systematic correlations between the $K^0_L\pi^0$ yields in this analysis and these additional $\mathcal{B}(K^0_L\pi^0)$ measurements

TABLE XI. External mixing measurements used to constrain r^2.

Parameter	Average (%)
$R_{\rm WS}$	0.409 ± 0.022 [33–35]
$R_{\rm M}$	0.0173 ± 0.0387 [36–39]

TABLE XII. External measurements of y and y' with associated measurements of r^2 and x'^2.

Parameter	Value (%)
y	0.662 ± 0.211 [6,40–46]
x	0.811 ± 0.334 [6,46]
r^2	0.339 ± 0.012 [4,7,47]
y'	0.34 ± 0.30 [4,7,47]
x'^2	0.006 ± 0.018 [4,7,47]

is taken into account. We also include the statistical correlation between $\mathcal{B}(K^0_L\pi^0)$ and $\mathcal{B}(K^0_S\pi^0)$; knowledge of the latter is required to correct for the effect of quantum correlations in the former.

Table X summarizes the external branching fraction inputs to the fit.

B. External mixing measurements

1. Information on r^2 from wrong-sign $D^0 \to K^+\pi^-$ and $D^0 \to K^{(*)+}\ell^-\nu_\ell$

Studies of wrong-sign $D^0 \to K^+\pi^-$ from other experiments provide information on r^2, y', and R_M. Without using D^0 decay times, these analyses are sensitive to the time-integrated wrong-sign rate ratio:

$$R_{WS} \equiv \frac{\Gamma(D^0 \to K^+\pi^-)}{\Gamma(\bar{D}^0 \to K^+\pi^-)} \tag{16}$$

$$= r^2 + ry' + R_M \tag{17}$$

$$= r^2 + \sqrt{r^2}y\cos\delta - \sqrt{r^2}x\sin\delta + \frac{x^2+y^2}{2}, \tag{18}$$

where Eq. (18) explicitly shows the dependence on the fit parameters r^2, y, $\cos\delta$, x^2, and $x\sin\delta$. By also measuring the decay times of the same D^0 candidates, these experiments can separate the three terms in Eq. (17) because each has a different proper time dependence:

$$\frac{dN}{dt} \propto e^{-\Gamma t}\left[r^2 + ry'\Gamma t + \frac{x'^2+y'^2}{4}(\Gamma t)^2\right]. \tag{19}$$

We use time-integrated R_{WS} measurements as a source of information on r^2, which is otherwise poorly determined in our analysis, as shown in Table XV. Constraining r^2 leads directly to improved precision on $\cos\delta$ because it always appears as $r\cos\delta$ in Table I. Extracting meaningful precision on r^2 from R_{WS} requires information on $x\sin\delta$ and x^2. When the external y and y' measurements described in Sec. IV B 2 are not included in the fit, $x\sin\delta$ is poorly determined, so we take $x\sin\delta$ to be zero. For x^2, which is also poorly determined in our analysis, we use R_M measurements from wrong-sign $D^0 \to K^{(*)+}\ell^-\nu_\ell$ rates. Table XI shows the input R_{WS} and semileptonic R_M measurements, which are uncorrelated with all other measurements and are entered directly into the fit.

2. Measurements of y and y'

By combining external measurements of y and y' with the CLEO-c measurement of $\cos\delta$, the fitter can extract $x\sin\delta$ via $x\sin\delta = y\cos\delta - y'$. In doing so, it accounts for the fact that y' is determined simultaneously with r^2 and R_M, which are also functions of the fit parameters, and that $\cos\delta$ and its uncertainty are correlated with y (as discussed below in Sec. VI).

External measurements of y come from two sources: comparison of D^0 decay times to CP eigenstates K^+K^- and $\pi^+\pi^-$ with decay times to the flavor eigenstate $K^-\pi^+$, and time-dependent Dalitz plot analysis of $D \to K^0_S\pi^+\pi^-$, which is sensitive to both x and y. The latter x and y measurements are essentially uncorrelated, but x provides information on y when combined with measurements of R_M.

For y', we use three sets of (CP-conserving) fit results from CLEO, Belle, and *BABAR*. Averages of these fits are shown in Table XII. The fit covariance matrices have been provided by the above collaborations and are also included in our analysis.

We note that, if we assume $x\sin\delta = 0$, the y and y' measurements in Table XII by themselves provide an independent measurement of $\cos\delta = (y' + x\sin\delta)/y = 0.52 \pm 0.49$, which is consistent with but less precise than the value found independently with CLEO-c data (see Section VI).

V. SYSTEMATIC UNCERTAINTIES

All uncertainties except statistical uncertainties on the measured yields are considered to be systematic in origin. Systematic uncertainties on the fit inputs are included directly in the covariance matrix given to the fitter, which propagates them to the fit parameters. Uncorrelated yield uncertainties are discussed above in Sec. III. Below, we summarize the sources of correlated uncertainty and the measurements to which they apply.

Final-state-dependent correlated systematic uncertainties, such as for tracking, particle identification (PID), and π^0 and K^0_S finding efficiencies are the dominant uncertainties for the branching fractions, but, as discussed in Ref. [19], when no external measurements are included,

TABLE XIII. Correlated, fractional efficiency systematic uncertainties and the schemes for applying them in the data branching fraction fit.

Source	Uncertainty (%)	Scheme
Track finding	0.3	per track
$K^\pm$ hadronic interactions	0.6	per $K^\pm$
K^0_S finding	1.9	per K^0_S
π^0 finding	4.0	per π^0
η finding	4.0	per η
dE/dx and RICH	0.3	per $\pi^\pm$ PID cut
dE/dx and RICH	0.3	per $K^\pm$ PID cut
EID	1.0	per $e^\pm$

TABLE XIV. Correlated, mode-dependent fractional systematic uncertainties in percent for STs. An asterisk (*) marks those uncertainties that are correlated among modes. The schemes by which these uncertainties are applied to DTs are also given, along with the fractional DT uncertainty, $\lambda_{\rm DT}$, on mode $\{A, B\}$ for ST uncertainties of α on mode A and β on mode B.

	ΔE	ISR *	FSR *	Lepton Veto *	Other	
$K^{\mp}\pi^{\pm}$	0.5	0.5	1.2	0.5		
K^+K^-	0.9	0.5	0.8	0.4	0.5	$K^{\pm}\cos\theta$ cut
$\pi^+\pi^-$	1.9	0.5	1.7	3.2		
$K^0_S\pi^0\pi^0$	2.6	0.5			1.5	K^0_S daughter PID
					0.7	resonant substructure
$K^0_S\pi^0$	0.9	0.5				
$K^0_S\eta$	5.5	0.5			0.3	η mass cut
					0.7	$\mathcal{B}(\eta\to\gamma\gamma)$ [28]
$K^0_S\omega$	1.2	0.5	0.8		1.4	ω mass cut
					0.8	$\mathcal{B}(\omega\to\pi^+\pi^-\pi^0)$ [28]
$Xe\nu_e$		0.5	0.3		2.0	spectrum extrapolation
					0.7	multiple $e^{\pm}$ candidates
$K^0_L\pi^0$		0.5			0.7	background subtraction
					0.3	extra track veto
					1.4	signal shape
					1.6	extra π^0 veto
					0.5	η veto
Scheme	per D	per yield	per D	per ST	per D	
$\lambda_{\rm DT}$	$\sqrt{\alpha^2+\beta^2}$	$(\alpha+\beta)/2$	$\alpha+\beta$	0	$\sqrt{\alpha^2+\beta^2}$	

they cancel in the DCS and mixing parameters. However, external measurements are, in general, not subject to the same correlated effects as our measured yields. Thus, while these external measurements reduce the statistical uncertainties on y and $\cos\delta$, they also introduce sensitivity to correlated uncertainties, and they increase the systematic uncertainties somewhat.

TABLE XV. Results from the fit with external inputs from Table X, but not Tables XI or XII. Uncertainties are statistical and systematic, respectively. Charge-averaged D^0 branching fractions are denoted by final state.

Parameter	Fitted Value
$\mathcal{N}(10^6)$	$1.062 \pm 0.024 \pm 0.011$
$y(10^{-3})$	$-52 \pm 60 \pm 17$
$r^2(10^{-3})$	$-24 \pm 16 \pm 12$
$r\cos\delta$	$0.089 \pm 0.036 \pm 0.009$
$R_{\rm M}(10^{-3})$	$2.0 \pm 1.2 \pm 1.2$
$rx\sin\delta(10^{-3})$	0 (fixed)
$\mathcal{B}(K^-\pi^+)(\%)$	$3.81 \pm 0.05 \pm 0.06$
$\mathcal{B}(K^-K^+)(10^{-3})$	$3.86 \pm 0.06 \pm 0.06$
$\mathcal{B}(\pi^-\pi^+)(10^{-3})$	$1.37 \pm 0.02 \pm 0.03$
$\mathcal{B}(K^0_S\pi^0\pi^0)(10^{-3})$	$8.27 \pm 0.45 \pm 0.41$
$\mathcal{B}(K^0_S\pi^0)(\%)$	$1.13 \pm 0.03 \pm 0.03$
$\mathcal{B}(K^0_S\eta)(10^{-3})$	$4.36 \pm 0.15 \pm 0.27$
$\mathcal{B}(K^0_S\omega)(\%)$	$1.10 \pm 0.04 \pm 0.05$
$\mathcal{B}(X^-e^+\nu_e)(\%)$	$6.35 \pm 0.19 \pm 0.18$
$\mathcal{B}(K^0_L\pi^0)(\%)$	$1.02 \pm 0.03 \pm 0.02$
$\chi^2_{\rm fit}/{\rm ndof}$	26.1/44

In Table XIII, we list the correlated systematic uncertainties on reconstruction and PID efficiencies for final state particles, determined as Refs. [27,52] describe. We also apply the efficiency corrections given in Refs. [27,52] with the following modifications. For π^0 finding efficiency, we adjust the relative correction to -3.3% and inflate the systematic uncertainty to 4.0% to account for our inclusion of signal modes with more energetic π^0s than in Ref. [27]. For η finding efficiency, the relative correction appropriate for our selection criteria is -6.5% with an uncertainty of 4.0%. For K^0_S finding efficiency, we include additional contributions of 0.3% and 0.4% for the flight significance and invariant mass requirements. We also include uncertainties on peaking background branching fractions, shown in Table IX. The signal and background efficiencies listed in this paper include the corrections discussed above.

Table XIV shows mode-dependent uncertainties. Most are assessed by relaxing selection requirements and noting the resultant change in efficiency-corrected yield. We compute each of these uncertainties as the quadrature sum of the yield shift and its statistical uncertainty, where the latter quantity accounts for the large correlation between the two yields.

The effect of modeling of the $K^0_S\pi^0\pi^0$ resonant substructure on the efficiency is determined by reweighting the simulated events according to the substructure observed in data and recomputing the efficiency. We assign an uncertainty for the modeling of multiple electron candidates by

TABLE XVI. Correlation coefficients (%) for the fit in Table XV using both statistical and systematic uncertainties.

	y	r^2	$r\cos\delta$	$R_{\rm M}$	$K^-\pi^+$	K^-K^+	$\pi^-\pi^+$	$K^0_S\pi^0\pi^0$	$K^0_S\pi^0$	$K^0_S\eta$	$K^0_S\omega$	$X^-e^+\nu_e$	$K^0_L\pi^0$
$\mathcal{N}$	−13	−37	−3	5	−44	−60	−46	−17	−46	−27	−28	−17	37
y		−32	−83	−6	−23	12	7	−0	−4	2	−3	30	7
r^2			39	1	−16	7	−6	8	23	11	20	29	−20
$r\cos\delta$				6	23	−3	−1	12	21	4	13	−21	−22
$R_{\rm M}$					−9	−3	−3	−0	−1	−1	−1	−2	1
$K^-\pi^+$						72	74	10	27	14	21	−16	−22
K^-K^+							73	12	31	18	24	9	−25
$\pi^-\pi^+$								9	25	14	20	−0	−19
$K^0_S\pi^0\pi^0$									64	15	46	3	−37
$K^0_S\pi^0$										31	59	8	−66
$K^0_S\eta$											20	5	−22
$K^0_S\omega$												9	−38
$X^-e^+\nu_e$													−5

taking the difference between multiple candidate rates in simulated events and data. The efficiency of the extra track, π^0, and η vetos in $K^0_L\pi^0$ modes is studied by comparing the frequency of these extra particles between simulated events and data. For semileptonic decays, we extrapolate the observed electron momentum spectrum below 200 MeV/c based on the simulation. By sampling different form factor models used in the simulation, we estimate a relative uncertainty of 25% on this extrapolation.

In our simulation, final state radiation (FSR) is generated by PHOTOS [53]. We measure efficiencies with and without FSR generation and assign 30% of the difference as a systematic uncertainty [27]. We also include a contribution corresponding to the change in efficiency when PHOTOS does and does not model interference among the radiated photons.

Unlike FSR, initial state radiation (ISR) coherently shifts both M values upward in a signal DT. So, mismodeling of ISR would affect ST and DT efficiencies by the same fraction. Based on a study of excluding events in the ISR region ($M > 1.87$ GeV/c^2), we assign a conservative 0.5% uncertainty to all yields.

VI. FIT RESULTS

We tested the analysis technique with the full simulated sample of uncorrelated $D^0\bar{D}^0$ decays that was filtered to leave a 40% subset of events that mimic the effect of quantum correlations. The effective luminosity of this subset is 15 times that of the data sample. The fit results showed satisfactory agreement with the input values, taking into account the statistical correlation between the signal efficiencies (measured in the full simulated sample) and the signal yields (measured in the 40% subset).

In Table XV, we first show the results of a data fit that includes external branching fraction measurements from Table X, but not the external $R_{\rm WS}$ and $R_{\rm M}$ measurements in Table XI. The corresponding correlation matrix for the fit parameters is given in Table XVI. Because r^2 has a large uncertainty and a negative central value, we cannot extract $\cos\delta$; instead, we quote $r\cos\delta$. Also, we fit for $R_{\rm M}$ instead of x^2.

In order to control the uncertainty on $\cos\delta$, we include in our standard fit both external branching fractions from Table X as well as external $R_{\rm WS}$ and $R_{\rm M}$ measurements from Table XI. In this fit, shown in Table XVII, we obtain a first measurement of $\cos\delta$, consistent with being at the boundary of the physical region and with a precision that is dominated by the CLEO-c $\{K\pi, S_\pm\}$ yield measurements. Our value of y is consistent with the world average of $0.006\,62 \pm 0.002\,11$ (see Table XII). For this standard fit, we assume $x\sin\delta = 0$, and the associated systematic uncertainty is ± 0.03 for $\cos\delta$ and negligible for all other parameters. The correlation matrix for this standard fit is shown in Table XVIII. Our branching fraction results do not supersede other CLEO-c measurements.

The likelihood curve for $\cos\delta$ is obtained by repeating this fit at fixed values of $\cos\delta$ and recording the change in

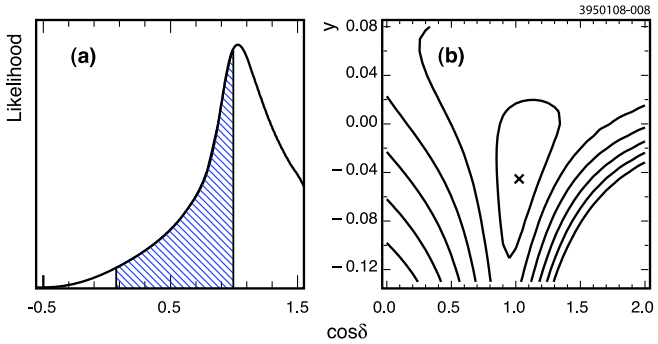

FIG. 6 (color online). Standard fit likelihood including both statistical and systematic uncertainties for $\cos\delta$ (a), and simultaneous likelihood for $\cos\delta$ and y (b) shown as contours in increments of 1σ, where $\sigma = \sqrt{\Delta\chi^2}$. The hatched region contains 95% of the area in the physical region.

TABLE XVII. Results from the standard fit (with inputs from Tables X and XI) and the extended fit (with inputs from Tables X, XI, and XII). Uncertainties are statistical and systematic, respectively. Charge-averaged D^0 branching fractions are denoted by final state.

Parameter	Standard fit	Extended fit
$\mathcal{N}(10^6)$	$1.042 \pm 0.021 \pm 0.010$	$1.042 \pm 0.021 \pm 0.010$
$y(10^{-3})$	$-45 \pm 59 \pm 15$	$6.5 \pm 0.2 \pm 2.1$
$r^2(10^{-3})$	$8.0 \pm 6.8 \pm 1.9$	$3.44 \pm 0.01 \pm 0.09$
$\cos\delta$	$1.03 \pm 0.19 \pm 0.06$	$1.10 \pm 0.35 \pm 0.07$
$x^2(10^{-3})$	$-1.5 \pm 3.6 \pm 4.2$	$0.06 \pm 0.01 \pm 0.05$
$x\sin\delta(10^{-3})$	0 (fixed)	$4.4 \pm 2.4 \pm 2.9$
$K^-\pi^+(\%)$	$3.78 \pm 0.05 \pm 0.05$	$3.78 \pm 0.05 \pm 0.05$
$K^-K^+(10^{-3})$	$3.87 \pm 0.06 \pm 0.06$	$3.88 \pm 0.06 \pm 0.06$
$\pi^-\pi^+(10^{-3})$	$1.36 \pm 0.02 \pm 0.03$	$1.36 \pm 0.02 \pm 0.03$
$K^0_S\pi^0\pi^0(10^{-3})$	$8.34 \pm 0.45 \pm 0.42$	$8.35 \pm 0.44 \pm 0.42$
$K^0_S\pi^0(\%)$	$1.14 \pm 0.03 \pm 0.03$	$1.14 \pm 0.03 \pm 0.03$
$K^0_S\eta(10^{-3})$	$4.42 \pm 0.15 \pm 0.28$	$4.42 \pm 0.15 \pm 0.28$
$K^0_S\omega(\%)$	$1.12 \pm 0.04 \pm 0.05$	$1.12 \pm 0.04 \pm 0.05$
$X^-e^+\nu_e(\%)$	$6.54 \pm 0.17 \pm 0.17$	$6.59 \pm 0.16 \pm 0.16$
$K^0_L\pi^0(\%)$	$1.01 \pm 0.03 \pm 0.02$	$1.01 \pm 0.03 \pm 0.02$
$\chi^2_{\rm fit}/{\rm ndof}$	30.1/46	55.3/57

minimum χ^2. We then compute $\mathcal{L} = e^{-(\chi^2-\chi^2_{\rm min})/2}$, which is shown in Fig. 6(a). It is highly non-Gaussian, so we assign asymmetric uncertainties by finding the values of $\cos\delta$ where $\Delta\chi^2 = 1$ to obtain $\cos\delta = 1.03^{+0.31}_{-0.17} \pm 0.06$. For values of $|\cos\delta| < 1$, we also compute $\mathcal{L}$ as a function of $|\delta|$, and we integrate these curves within the physical region to obtain 95% confidence level limits of $\cos\delta > 0.07$ and $|\delta| < 75°$.

The asymmetric uncertainties on $\cos\delta$ quoted above still do not fully capture the nonlinearity of the likelihood. This nonlinearity stems from the use of r^2 to convert $r\cos\delta$ into $\cos\delta$, which causes the uncertainty on $\cos\delta$ to scale roughly like $1/r$. Because r^2 is obtained from $R_{\rm WS}$ via Eq. (18), an upward shift in y lowers the derived value of r^2 (for positive $r\cos\delta$). As a result, the uncertainty on $\cos\delta$ increases with more positive y, as shown in Fig. 6(b). A second, smaller effect is that the sign of the correlation between r^2 and $r\cos\delta$ is given by the sign of y. When y is positive, r^2 and $r\cos\delta$ are anticorrelated, which tends to inflate the uncertainty on $\cos\delta$.

We also perform an extended fit that determines $x\sin\delta$ by including previous measurements of y and y'. Table XVII shows the results of this fit, which incorporates all external measurements, from Tables X, XI, and XII. The correlation matrix for the extended fit is given in Table XIX. The resultant value of y includes the CLEO-c measurement from the standard fit, but the precision is dominated by the external y measurements. The overall

TABLE XVIII. Correlation coefficients (%) for the standard fit in Table XVII using both statistical and systematic uncertainties.

	y	r^2	$\cos\delta$	x^2	$K^-\pi^+$	K^-K^+	$\pi^-\pi^+$	$K^0_S\pi^0\pi^0$	$K^0_S\pi^0$	$K^0_S\eta$	$K^0_S\omega$	$X^-e^+\nu_e$	$K^0_L\pi^0$
$\mathcal{N}$	−11	8	−22	−10	−65	−61	−53	−15	−42	−24	−23	2	33
y		−99	49	99	−20	10	6	−0	−6	1	−4	30	7
r^2			−38	−99	21	−8	−5	3	9	0	6	−30	−11
$\cos\delta$				50	2	15	12	17	22	8	13	13	−22
x^2					−20	10	6	−0	−6	1	−4	30	7
$K^-\pi^+$						80	77	12	35	19	28	−5	−28
K^-K^+							74	11	30	19	28	−6	−28
$\pi^-\pi^+$								10	26	15	22	1	−21
$K^0_S\pi^0\pi^0$									64	14	46	0	−36
$K^0_S\pi^0$										29	57	−2	−65
$K^0_S\eta$											18	−0	−21
$K^0_S\omega$												1	−36
$X^-e^+\nu_e$													2

TABLE XIX. Correlation coefficients (%) for the extended fit in Table XVII using both statistical and systematic uncertainties.

	y	r^2	$\cos\delta$	x^2	$x\sin\delta$	$K^-\pi^+$	K^-K^+	$\pi^-\pi^+$	$K^0_S\pi^0\pi^0$	$K^0_S\pi^0$	$K^0_S\eta$	$K^0_S\omega$	$X^-e^+\nu_e$	$K^0_L\pi^0$
$\mathcal{N}$	0	−0	−19	0	−12	−69	−61	−53	−15	−43	−24	−23	5	34
y		13	−6	−6	69	0	0	−0	0	−0	−0	−0	1	0
r^2			−5	26	37	−0	0	−0	0	0	0	0	0	−0
$\cos\delta$				−1	56	14	12	10	20	29	9	17	1	−30
x^2					19	−0	−0	−0	−0	−0	−0	−0	−0	0
$x\sin\delta$						8	8	6	13	18	5	11	1	−18
$K^-\pi^+$							84	80	12	34	19	28	1	−27
K^-K^+								74	11	31	17	23	1	−24
$\pi^-\pi^+$									10	27	15	22	−0	−21
$K^0_S\pi^0\pi^0$										64	14	46	1	−36
$K^0_S\pi^0$											29	57	1	−65
$K^0_S\eta$												18	−0	−21
$K^0_S\omega$													3	−36
$X^-e^+\nu_e$														−1

uncertainty on $\cos\delta$ increases to ± 0.36 because of the $R_{\rm WS}$ measurement, as discussed above. However, unlike the standard fit, the likelihood for $\cos\delta$ shown in Fig. 7(a) is nearly Gaussian. For $x\sin\delta$, we assign asymmetric uncertainties resulting in $x\sin\delta = (4.4^{+2.7}_{-1.8} \pm 2.9) \times 10^{-3}$. By repeating the fit at various simultaneously fixed values of $\cos\delta$ and $\sin\delta$, we also determine $\delta = (22^{+11+9}_{-12-11})^\circ$. The corresponding 95% confidence level intervals within the physical region are $\cos\delta > 0.39$, $x\sin\delta \in [0.002, 0.014]$, and $\delta \in [-7^\circ, +61^\circ]$. Performing this extended fit with y, x^2, and $x\sin\delta$ fixed to zero results in a change in χ^2 of 25.1, or a significance of 5.0σ.

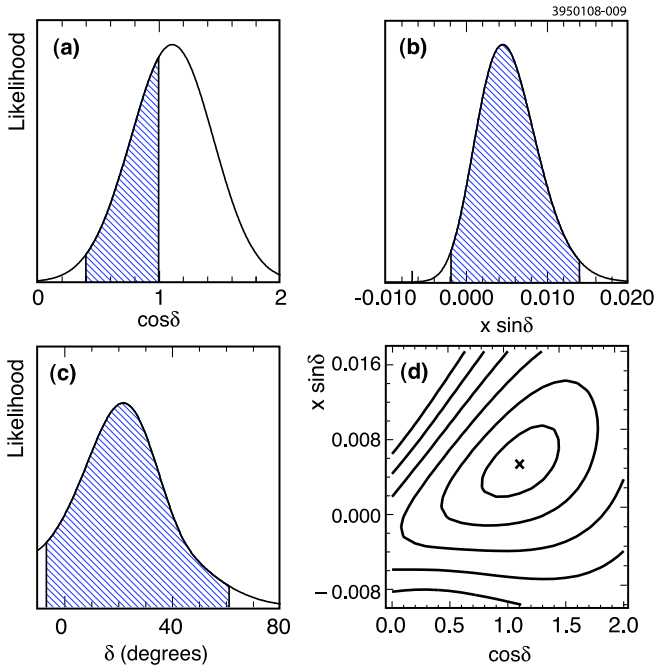

FIG. 7 (color online). Extended fit likelihood including both statistical and systematic uncertainties for $\cos\delta$ (a), $x\sin\delta$ (b), δ (c), and simultaneous likelihood for $\cos\delta$ and $x\sin\delta$ (d) shown as contours in increments of 1σ, where $\sigma = \sqrt{\Delta\chi^2}$. The hatched regions contain 95% of the area in the physical regions. For δ, the fit fails to converge beyond the limits of the plot.

In the standard fit, the large correlation between y and r^2 originates in the use of the $R_{\rm WS}$ measurement in Table XI to provide information on r^2. Using Eq. (18), one sees that the precision on r^2 is driven by the precision on y. Hence, for positive $r\cos\delta$, r^2 and y are negatively correlated. Consequently, the $\cos\delta$ value obtained by dividing $r\cos\delta$ by $\sqrt{r^2}$ is positively correlated with y. In the extended fit, these correlations are broken by the precise external measurements of y in Table XII, and the weak negative correlation between $\cos\delta$ and y results from Eqs. (10) and (11).

We assess the fit's sensitivity to the assumed quantum correlation parameters in the peaking background subtractions by varying these parameters over their full allowed ranges. We find excursions of less than 1×10^{-4} in y and 0.003 in $\cos\delta$ for both the standard and extended fits. We assign a systematic uncertainty, included in Table XVII given by the size of these shifts.

A. Analysis of input information

In this section, we probe the power of the individual fit inputs or groups of fit inputs by removing them from the standard fit one by one. We define the weight (or information) that each input contributes to fit parameter λ to be the fractional change in $1/\sigma^2_\lambda$ when it is removed from the fit:

$$I_\lambda \equiv \frac{1/\sigma^2_\lambda(\text{new}) - 1/\sigma^2_\lambda(\text{standard})}{1/\sigma^2_\lambda(\text{standard})}. \qquad (20)$$

TABLE XX. Effect of removing inputs from the standard fit. For each input and fit parameter combination, we report the significance of the shift in central value $\mathcal{S}_\lambda$ and the fractional information content I_λ. In cases where I_λ is negative, we do not report the shift significance.

Removed input	$\mathcal{S}_y$	I_y	$\mathcal{S}_{\cos\delta}$	$I_{\cos\delta}$
Single tag yields				
$K^-\pi^+$	$+0.1\sigma$	0%	-0.0σ	0%
$K^+\pi^-$	$+0.2\sigma$	0%	-0.0σ	1%
K^+K^-	$+1.1\sigma$	6%	$+0.4\sigma$	41%
$\pi^+\pi^-$	$+0.6\sigma$	1%	$+0.2\sigma$	11%
$K^0_S\pi^0\pi^0$	$+0.5$	2%	$+0.4\sigma$	23%
$K^0_S\pi^0$	$+1.1\sigma$	14%	$+0.5\sigma$	72%
$K^0_S\eta$	-2.8σ	0%	⋯	-31%
$K^0_S\omega$	-2.5σ	2%	⋯	-46%
Double tag yields				
$K^\pm\pi^\mp$, $K^\pm\pi^\mp$	$+0.1\sigma$	1%	$+0.1\sigma$	8%
$K^-\pi^+$, $K^+\pi^-$	⋯	-0%	⋯	-2%
$K\pi$, S_+	⋯	-0%	-0.0σ	48%
$K\pi$, S_-	-0.1σ	0%	$+0.0\sigma$	38%
S_+, S_-	$+0.9\sigma$	0%	$+0.2\sigma$	11%
$K\pi$, $e^\pm$	-0.0σ	11%	-0.1σ	1%
S'_+, $e^\pm$	-0.3σ	37%	⋯	-19%
S_-, $e^\pm$	-0.9σ	54%	⋯	-135%
$K^0_L\pi^0$, $K\pi$	⋯	-3%	-1.3σ	14%
$K^0_L\pi^0$, S_-	⋯	-0%	$+0.2\sigma$	5%
External or other CLEO-c (*) inputs				
$R_{\rm WS}$, $R_{\rm M}$	-0.6σ	3%	⋯	100%
$\mathcal{B}(K^-\pi^+)$	-1.2σ	1%	⋯	-12%
$\mathcal{B}(K^+K^-)$	$+1.4\sigma$	3%	$+0.2\sigma$	29%
$\mathcal{B}(\pi^+\pi^-)$	⋯	-0%	⋯	-1%
$\mathcal{B}(K^0_S\pi^0)$	$+0.4\sigma$	1%	-0.2σ	3%
$\mathcal{B}(K^0_S\eta)$	$+1.4\sigma$	0%	$+0.0\sigma$	5%
$\mathcal{B}(K^0_S\omega)$	$+0.1\sigma$	0%	-0.3σ	0%
$\mathcal{B}(K^0_L\pi^0)^*$	⋯	-5%	-1.2σ	6%

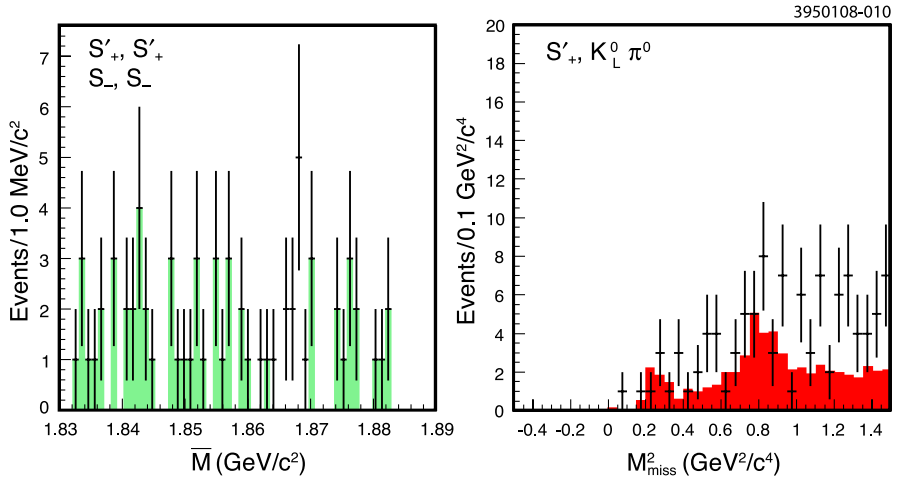

FIG. 8 (color online). Combined $\bar{M}$ distribution for fully reconstructed same-CP $\{S'_+, S'_+\}$ and $\{S_-, S_-\}$ DT modes and combined $M^2_{\rm miss}$ distribution for $\{S'_+, K^0_L\pi^0\}$ modes. Data are shown as points with error bars. For $\{S'_+, S'_+\}$ and $\{S_-, S_-\}$, the shaded histogram shows events outside the signal region. For $\{S'_+, K^0_L\pi^0\}$, the shaded histogram represents simulations of the peaking backgrounds $D^0 \to \pi^0\pi^0$, $K^0_S\pi^0$, $\eta\pi^0$, and $K^{*0}\pi^0$.

TABLE XXI. Same-*CP* double tag yields and efficiencies included in the *C*-even-allowed fit.

Mode	Yield	Efficiency (%)
K^+K^-, K^+K^-	$-2.1 \pm 1.5 \pm 3.1$	32.4 ± 1.7
K^+K^-, $\pi^+\pi^-$	$0.9 \pm 1.6 \pm 1.1$	38.9 ± 2.2
K^+K^-, $K^0_S\pi^0\pi^0$	$0.0 \pm 1.0 \pm 0.0$	6.6 ± 0.5
$\pi^+\pi^-$, $\pi^+\pi^-$	$1.2 \pm 2.8 \pm 4.8$	44.9 ± 5.1
$\pi^+\pi^-$, $K^0_S\pi^0\pi^0$	$1.0 \pm 1.0 \pm 0.0$	9.2 ± 1.0
$K^0_S\pi^0\pi^0$, $K^0_S\pi^0\pi^0$	$0.0 \pm 1.0 \pm 0.0$	1.5 ± 0.2
$K^0_S\pi^0$, $K^0_S\pi^0$	$0.0 \pm 1.0 \pm 0.0$	8.9 ± 0.5
$K^0_S\pi^0$, $K^0_S\eta$	$0.0 \pm 1.0 \pm 0.0$	2.9 ± 0.3
$K^0_S\pi^0$, $K^0_S\omega$	$1.0 \pm 1.0 \pm 0.0$	3.3 ± 0.2
$K^0_S\eta$, $K^0_S\eta$	$0.0 \pm 1.0 \pm 0.0$	0.7 ± 0.4
$K^0_S\eta$, $K^0_S\omega$	$0.0 \pm 1.0 \pm 0.0$	1.0 ± 0.2
$K^0_S\omega$, $K^0_S\omega$	$1.0 \pm 1.0 \pm 0.0$	1.5 ± 0.2
$K^0_L\pi^0$, K^+K^-	$1.7 \pm 2.1 \pm 0.0$	28.2 ± 0.1
$K^0_L\pi^0$, $\pi^+\pi^-$	$4.3 \pm 2.4 \pm 0.0$	38.5 ± 0.1
$K^0_L\pi^0$, $K^0_S\pi^0\pi^0$	$2.7 \pm 2.3 \pm 0.0$	6.4 ± 0.1

Because of the aforementioned nonlinearities, removing an input from the fit can result in a σ_λ that is *smaller* than the standard value, leading to negative I_λ.

Table XX shows I_λ for $\lambda = y$ and $\cos\delta$. When $I_\lambda > 0$, we also calculate the significance of the shift to be $\mathcal{S}_\lambda \equiv \Delta\lambda/\sqrt{\sigma^2_\lambda(\text{standard}) - \sigma^2_\lambda(\text{new})}$, where the minus sign accounts for the correlation between the two values of λ.

As expected from Eqs. (8), (9), and (12), information about y comes primarily from the $\{S_\pm, e\}$ DT yields, which supply 91% of the statistical power. In addition, the $\{K\pi, e\}$ yields provide the normalizing semileptonic branching fraction, and $S_\pm$ ST yields provide $\mathcal{N}\mathcal{B}_{S_\pm}$. Because y is determined from ratios of these quantities, a meaningful measurement depends on the simultaneous presence of various combinations of inputs. For instance, removing the $S_\pm$ ST yields would also reduce the power of the $\{S_\pm, e\}$ DT yields because, then, Eq. (8) cannot be used. Table XX does not account for such double-counting of information; it simply shows I_λ as each individual input is removed from the fit. For this reason, the sum of all I_y exceeds 100%.

This effect is even more pronounced with $\cos\delta$. As demonstrated in Eqs. (10) and (13), almost all the information about $r\cos\delta$ is contained in the $\{K\pi, S_\pm\}$ DT yields, but only when they are combined with the $\mathcal{B}_{S_\pm}$ estimates provided by the $S_\pm$ ST yields. Furthermore, in order to obtain $\cos\delta$ from $r\cos\delta$, we rely on the inputs from Table XI, which therefore have $I_{\cos\delta} = 1$. If either $\{K\pi, S_+\}$ or $\{K\pi, S_-\}$ yields are removed, then the asymmetries in Eqs. (10) and (13) cannot be formed. However, $r\cos\delta$ can still be obtained with knowledge of $\mathcal{N}\mathcal{B}_{K^-\pi^+}\mathcal{B}_{S_\pm}$, which comes from other inputs in the fit.

A striking example of nonlinearities in the fit occurs when $\{S_-, e^\pm\}$ double tags are removed. Doing so causes y to fluctuate downward, which, in turn, *lowers* the uncertainty on $\cos\delta$, as discussed above. As a result, $\{S_-, e^\pm\}$ double tags appear to have large *negative* information content.

In performing this exercise, we also test for anomalous inputs that bias the fit results with undue weight. As Table XX shows, we find no evidence of instability from our choice of fit inputs.

TABLE XXII. Comparison of *C*-odd and *C*-even yields, normalized by $\mathcal{N}A_i^2$ for ST modes i and by $\mathcal{N}A_i^2A_j^2$ for DT modes $\{i, j\}$, to leading order in x, y, and r^2, with $y' \equiv y\cos\delta - x\sin\delta$ and $\tilde{y} \equiv y\cos\delta + x\sin\delta$. Charge conjugate modes are implied.

Mode	R_{C-}	R_{C+}
$K^-\pi^+$	$1 + 2ry\cos\delta + r^2$	$1 + 2ry\cos\delta + r^2$
S_+	$2(1 - y)$	$2(1 - y)$
S_-	$2(1 + y)$	$2(1 + y)$
$K^-\pi^+$, $K^-\pi^+$	R_M	$2r(r + y')$
$K^-\pi^+$, $K^+\pi^-$	$1 + 2r^2(1 - 2\cos^2\delta)$	$1 - 2r^2(1 - 2\cos^2\delta) + 4r\tilde{y}$
$K^-\pi^+$, S_+	$1 + 2r\cos\delta + r^2$	$[1 - 2r\cos\delta + r^2](1 - 2y)$
$K^-\pi^+$, S_-	$1 - 2r\cos\delta + r^2$	$[1 + 2r\cos\delta + r^2](1 + 2y)$
$K^-\pi^+$, e^-	1	$1 + 2r\tilde{y}$
S_+, S_+	0	$2(1 - 2y)$
S_-, S_-	0	$2(1 + 2y)$
S_+, S_-	4	0
S_+, e^-	1	$1 - 2y$
S_-, e^-	1	$1 + 2y$

TABLE XXIII. Results from the fits allowing for a C-even component in the initial state, with inputs from Table XXI. Uncertainties are statistical and systematic, respectively. We also give the shifts in the fit results with respect to the nominal fits.

Parameter	Standard, C-even allowed	Shift	Extended, C-even allowed	Shift
$\mathcal{N}_{C-}(10^6)$	$1.044 \pm 0.029 \pm 0.017$	$+0.002$	$1.044 \pm 0.030 \pm 0.017$	$+0.002$
$\mathcal{N}_{C+}/\mathcal{N}_{C-}(10^{-3})$	$-1.5 \pm 23.0 \pm 2.2$	—	$-1.4 \pm 23.6 \pm 1.9$	$\cdots$
$y(10^{-3})$	$-46 \pm 59 \pm 16$	-0.2	$6.5 \pm 0.2 \pm 2.1$	-0.0
$r^2(10^{-3})$	$8.0 \pm 6.8 \pm 1.9$	$+0.008$	$3.44 \pm 0.01 \pm 0.09$	-0.000
$\cos\delta$	$1.02 \pm 0.19 \pm 0.06$	-0.003	$1.10 \pm 0.35 \pm 0.07$	-0.005
$x^2(10^{-3})$	$-1.5 \pm 4.1 \pm 3.8$	-0.2	$0.06 \pm 0.01 \pm 0.05$	$+0.01$
$x\sin\delta(10^{-3})$	0 (fixed)	$\cdots$	$4.4 \pm 2.4 \pm 2.9$	-0.04
$\mathcal{B}(K^-\pi^+)(\%)$	$3.78 \pm 0.05 \pm 0.05$	-0.001	$3.78 \pm 0.05 \pm 0.05$	-0.001
$\mathcal{B}(K^-K^+)(10^{-3})$	$3.87 \pm 0.06 \pm 0.06$	$+0.001$	$3.88 \pm 0.06 \pm 0.06$	$+0.001$
$\mathcal{B}(\pi^-\pi^+)(10^{-3})$	$1.36 \pm 0.02 \pm 0.03$	-0.000	$1.36 \pm 0.02 \pm 0.03$	-0.000
$\mathcal{B}(K^0_S\pi^0\pi^0)(10^{-3})$	$8.33 \pm 0.45 \pm 0.42$	-0.011	$8.34 \pm 0.44 \pm 0.42$	-0.011
$\mathcal{B}(K^0_S\pi^0)(\%)$	$1.14 \pm 0.03 \pm 0.03$	-0.001	$1.14 \pm 0.03 \pm 0.03$	-0.001
$\mathcal{B}(K^0_S\eta)(10^{-3})$	$4.42 \pm 0.15 \pm 0.28$	-0.002	$4.41 \pm 0.15 \pm 0.28$	-0.002
$\mathcal{B}(K^0_S\omega)(\%)$	$1.11 \pm 0.04 \pm 0.05$	-0.006	$1.11 \pm 0.04 \pm 0.05$	-0.006
$\mathcal{B}(X^-e^+\nu_e)(\%)$	$6.54 \pm 0.17 \pm 0.17$	-0.001	$6.59 \pm 0.16 \pm 0.16$	-0.001
$\mathcal{B}(K^0_L\pi^0)(\%)$	$1.01 \pm 0.03 \pm 0.02$	$+0.000$	$1.01 \pm 0.03 \pm 0.02$	$+0.000$
$\chi^2_{\rm fit}$/ndof	34.1/59		59.3/71	

B. Purity of C-odd initial state

The purity of the C-odd $D^0\bar{D}^0$ initial state may be diluted by a radiated photon, which would reverse the C eigenvalue of the $D^0\bar{D}^0$ system and thus bias the fit results. ISR, FSR, and bremsstrahlung photon emission are benign because they do not alter the relative angular momentum between the D^0 and $\bar{D}^0$, occurring either before the $D^0\bar{D}^0$ are formed or after they decay. One problematic process would be photon radiation from the $\psi(3770)$, resulting in a virtual 0^+ state that then decays to $D^0\bar{D}^0$. This channel is suppressed, as there are no nearby 0^+ states available. Another possible contribution would be $\psi(3770)$ decay to a virtual $D^{*0}\bar{D}^0$, which subsequently decays to $D^0\bar{D}^0\gamma$. Theoretical estimates of these amplitudes indicate a $\psi(3770) \to D^0\bar{D}^0\gamma$ branching fraction of less than 10^{-8} [54].

We verify the absence of this effect in data by searching for same-CP DT signals, which would be maximally enhanced for the C-even configuration. As shown in Fig. 8 and Table XXI, all such modes have yields consistent with zero. To determine the C-even fraction of the $D^0\bar{D}^0$ sample, $\mathcal{N}_{C+}/\mathcal{N}_{C-}$, we perform a variant of the standard and extended fits that include the 15 same-CP DT yields and efficiencies shown in Table XXI. We then express each yield as a sum of C-odd and C-even contributions: $N_{ij} = \mathcal{N}_{C-}A_i^2A_j^2R_{C-} + \mathcal{N}_{C+}A_i^2A_j^2R_{C+}$, where R_{C-} and R_{C+} are the functions of y, r, $\cos\delta$, and $x\sin\delta$ given in Table XXII. The results of these fits are shown in Table XXIII. The C-even fraction is found to be consistent with zero, with an uncertainty of 2.4%, and shifts of the fit parameters from the nominal fit results are negligible compared to the systematic uncertainties already assigned.

VII. SUMMARY

We employ a double tagging technique with quantum-correlated $D^0\bar{D}^0$ decays at the $\psi(3770)$ to perform a first measurement of $\cos\delta = 1.03^{+0.31}_{-0.17} \pm 0.06$, where the uncertainties are statistical and systematic, respectively. Within the physical region, we find $|\delta| < 75^\circ$ at the 95% confidence level. By including external inputs on y and y' in the fit, we find an alternative value of $\cos\delta = 1.10 \pm 0.35 \pm 0.07$, as well as $x\sin\delta = (4.4^{+2.7}_{-1.8} \pm 2.9) \times 10^{-3}$ and $\delta = (22^{+11+9}_{-12-11})^\circ$.

ACKNOWLEDGMENTS

We thank Alexey Petrov, William Lockman, Alan Schwartz, Bostjan Golob, and Brian Petersen for helpful discussions. We gratefully acknowledge the effort of the CESR staff in providing us with excellent luminosity and running conditions. D. Cronin-Hennessy and A. Ryd thank the A. P. Sloan Foundation. This work was supported by the National Science Foundation, the U.S. Department of Energy, and the Natural Sciences and Engineering Research Council of Canada.

APPENDIX: CORRECTED YIELDS

For use by future experiments, we provide our efficiency-corrected, background-subtracted yields in Tables XXIV and XXV. The correlation matrix, including statistical and systematic uncertainties, for these yields appears in Tables XXVI, XXVII, XXVIII, XXIX, XXX, and XXXI.

TABLE XXIV. Efficiency-corrected, background-subtracted single tag and double tag yields input to the fits. Uncertainties are statistical and systematic combined.

Mode	Yield
$K^-\pi^+$	39 159 ± 743
$K^+\pi^-$	39 326 ± 742
K^+K^-	8279 ± 208
$\pi^+\pi^-$	2877 ± 145
$K^0_S\pi^0\pi^0$	18 759 ± 1731
$K^0_S\pi^0$	24 923 ± 1167
$K^0_S\eta$	10 078 ± 790
$K^0_S\omega$	23 903 ± 1581
$K^-\pi^+$, $K^-\pi^+$	3.1 ± 3.9
$K^-\pi^+$, $K^+\pi^-$	1460 ± 78
$K^-\pi^+$, K^+K^-	199 ± 25
$K^-\pi^+$, $\pi^+\pi^-$	53 ± 11
$K^-\pi^+$, $K^0_S\pi^0\pi^0$	393 ± 79
$K^-\pi^+$, $K^0_S\pi^0$	472 ± 55
$K^-\pi^+$, $K^0_S\eta$	131 ± 49
$K^-\pi^+$, $K^0_S\omega$	337 ± 76
$K^+\pi^-$, $K^+\pi^-$	2.6 ± 3.2
$K^+\pi^-$, K^+K^-	149 ± 21
$K^+\pi^-$, $\pi^+\pi^-$	53 ± 11
$K^+\pi^-$, $K^0_S\pi^0\pi^0$	409 ± 80
$K^+\pi^-$, $K^0_S\pi^0$	401 ± 51
$K^+\pi^-$, $K^0_S\eta$	145 ± 50
$K^+\pi^-$, $K^0_S\omega$	370 ± 77
K^+K^-, K^+K^-	−6.5 ± 10.6
K^+K^-, $\pi^+\pi^-$	2.3 ± 5.0
K^+K^-, $K^0_S\pi^0\pi^0$	−0.3 ± 15.0
K^+K^-, $K^0_S\pi^0$	224 ± 38
K^+K^-, $K^0_S\eta$	97 ± 38
K^+K^-, $K^0_S\omega$	285 ± 67
$\pi^+\pi^-$, $\pi^+\pi^-$	2.7 ± 12.4
$\pi^+\pi^-$, $K^0_S\pi^0\pi^0$	11 ± 11
$\pi^+\pi^-$, $K^0_S\pi^0$	67 ± 19
$\pi^+\pi^-$, $K^0_S\eta$	24 ± 18

TABLE XXV. Efficiency-corrected, background-subtracted single tag and double tag yields input to the fits. Uncertainties are statistical and systematic combined.

Mode	Yield
$\pi^+\pi^-$, $K^0_S\omega$	67 ± 27
$K^0_S\pi^0\pi^0$, $K^0_S\pi^0\pi^0$	−0.7 ± 65.8
$K^0_S\pi^0\pi^0$, $K^0_S\pi^0$	395 ± 121
$K^0_S\pi^0\pi^0$, $K^0_S\eta$	327 ± 168
$K^0_S\pi^0\pi^0$, $K^0_S\omega$	265 ± 159
$K^0_S\pi^0$, $K^0_S\pi^0$	−2.5 ± 11.0
$K^0_S\pi^0$, $K^0_S\eta$	−1.0 ± 33.5
$K^0_S\pi^0$, $K^0_S\omega$	5.7 ± 31.7
$K^0_S\eta$, $K^0_S\eta$	0 ± 141
$K^0_S\eta$, $K^0_S\omega$	−9.4 ± 98.1
$K^0_S\omega$, $K^0_S\omega$	47 ± 66
$X^+e^-\bar{\nu}_e$, $K^-\pi^+$	2488 ± 131
$X^+e^-\bar{\nu}_e$, K^-K^+	319 ± 62
$X^+e^-\bar{\nu}_e$, $\pi^-\pi^+$	97 ± 28
$X^+e^-\bar{\nu}_e$, $K^0_S\pi^0\pi^0$	418 ± 289
$X^+e^-\bar{\nu}_e$, $K^0_S\pi^0$	903 ± 119
$X^+e^-\bar{\nu}_e$, $K^0_S\eta$	349 ± 94
$X^+e^-\bar{\nu}_e$, $K^0_S\omega$	601 ± 202
$X^-e^+\nu_e$, $K^+\pi^-$	2653 ± 135
$X^-e^+\nu_e$, K^-K^+	261 ± 60
$X^-e^+\nu_e$, $\pi^-\pi^+$	79 ± 22
$X^-e^+\nu_e$, $K^0_S\pi^0\pi^0$	518 ± 190
$X^-e^+\nu_e$, $K^0_S\pi^0$	876 ± 103
$X^-e^+\nu_e$, $K^0_S\eta$	349 ± 110
$X^-e^+\nu_e$, $K^0_S\omega$	570 ± 200
$K^0_L\pi^0$, $K^-\pi^+$	516 ± 47
$K^0_L\pi^0$, $K^+\pi^-$	485 ± 46
$K^0_L\pi^0$, K^+K^-	−6.8 ± 7.8
$K^0_L\pi^0$, $\pi^+\pi^-$	7.1 ± 6.3
$K^0_L\pi^0$, $K^0_S\pi^0\pi^0$	10 ± 37
$K^0_L\pi^0$, $K^0_S\pi^0$	565 ± 75
$K^0_L\pi^0$, $K^0_S\eta$	154 ± 59
$K^0_L\pi^0$, $K^0_S\omega$	508 ± 105

TABLE XXVI. Correlation coefficients (%), with statistical and systematic uncertainties, for the efficiency-corrected, background-subtracted yields in Tables XXIV and XXV. Coefficients of 100% are represented by dots (···).

	$K^-\pi^+$	$K^+\pi^-$	K^+K^-	$\pi^+\pi^-$	$K^0_S\pi^0\pi^0$	$K^0_S\pi^0$	$K^0_S\eta$	$K^0_S\omega$	$K^-\pi^+$, $K^-\pi^+$	$K^-\pi^+$, $K^+\pi^-$	$K^-\pi^+$, K^+K^-	$K^-\pi^+$, $\pi^+\pi^-$	$K^-\pi^+$, $K^0_S\pi^0\pi^0$	$K^-\pi^+$, $K^0_S\pi^0$	$K^-\pi^+$, $K^0_S\eta$	$K^-\pi^+$, $K^0_S\omega$	$K^+\pi^-$, $K^+\pi^-$	$K^+\pi^-$, K^+K^-	$K^+\pi^-$, $\pi^+\pi^-$	$K^+\pi^-$, $K^0_S\pi^0\pi^0$	$K^+\pi^-$, $K^0_S\pi^0$	$K^+\pi^-$, $K^0_S\eta$	$K^+\pi^-$, $K^0_S\omega$
$K^-\pi^+$	···	88	56	46	3	7	4	18	0	58	21	16	9	14	6	15	−0	22	16	8	13	5	13
$K^+\pi^-$		···	56	46	3	7	4	18	−0	58	19	15	8	12	5	14	1	23	17	9	15	6	14
K^+K^-			···	25	2	5	3	10	0	34	24	9	5	8	3	8	0	26	9	5	9	3	8
$\pi^+\pi^-$				···	1	2	1	8	0	20	6	15	3	4	2	6	0	7	16	3	5	2	6
$K^0_S\pi^0\pi^0$					···	82	5	63	0	2	1	1	43	28	1	22	0	1	1	42	31	1	22
$K^0_S\pi^0$						···	10	70	0	4	1	1	38	35	3	25	0	2	1	37	38	3	24
$K^0_S\eta$							···	8	0	2	1	1	2	4	23	3	0	1	1	2	4	22	3
$K^0_S\omega$								···	0	12	4	4	30	26	3	37	0	4	4	30	28	3	36
$K^-\pi^+$, $K^-\pi^+$									···	−2	0	0	0	0	0	0	0	0	0	0	0	0	0

TABLE XXVI. (*Continued*)

	$K^-\pi^+$	$K^+\pi^-$	K^+K^-	$\pi^+\pi^-$	$K^0_S\pi^0\pi^0$	$K^0_S\pi^0$	$K^0_S\eta$	$K^0_S\omega$	$K^-\pi^+, K^-\pi^+$	$K^-\pi^+, K^+\pi^-$	$K^-\pi^+, K^+K^-$	$K^-\pi^+, \pi^+\pi^-$	$K^-\pi^+, K^0_S\pi^0\pi^0$	$K^-\pi^+, K^0_S\pi^0$	$K^-\pi^+, K^0_S\eta$	$K^-\pi^+, K^0_S\omega$	$K^+\pi^-, K^+\pi^-$	$K^+\pi^-, K^+K^-$	$K^+\pi^-, \pi^+\pi^-$	$K^+\pi^-, K^0_S\pi^0\pi^0$	$K^+\pi^-, K^0_S\pi^0$	$K^+\pi^-, K^0_S\eta$	$K^+\pi^-, K^0_S\omega$
$K^-\pi^+, K^+\pi^-$									⋯	13	11	5	8	4	9	−2	15	11	5	9	3	9
$K^-\pi^+, K^+K^-$										⋯	4	2	3	1	3	0	6	4	2	3	1	3
$K^-\pi^+, \pi^+\pi^-$											⋯	2	2	1	3	0	4	4	2	3	1	3
$K^-\pi^+, K^0_S\pi^0\pi^0$												⋯	14	1	11	0	2	2	19	15	1	11
$K^-\pi^+, K^0_S\pi^0$													⋯	2	10	0	3	2	14	14	2	10
$K^-\pi^+, K^0_S\eta$														⋯	2	0	1	1	1	2	5	2
$K^-\pi^+, K^0_S\omega$															⋯	0	4	3	11	11	2	13
$K^+\pi^-, K^+\pi^-$																⋯	0	0	0	0	0	0
$K^+\pi^-, K^+K^-$																	⋯	4	2	4	1	4
$K^+\pi^-, \pi^+\pi^-$																		⋯	2	3	1	3
$K^+\pi^-, K^0_S\pi^0\pi^0$																			⋯	15	1	11
$K^+\pi^-, K^0_S\pi^0$																				⋯	2	11
$K^+\pi^-, K^0_S\eta$																					⋯	1
$K^+\pi^-, K^0_S\omega$																						⋯

TABLE XXVII. Correlation coefficients (%), with statistical and systematic uncertainties, for the efficiency-corrected, background-subtracted yields in Tables XXIV and XXV.

	K^+K^-, K^+K^-	$K^+K^-, \pi^+\pi^-$	$K^+K^-, K^0_S\pi^0\pi^0$	$K^+K^-, K^0_S\pi^0$	$K^+K^-, K^0_S\eta$	$K^+K^-, K^0_S\omega$	$\pi^+\pi^-, \pi^+\pi^-$	$\pi^+\pi^-, K^0_S\pi^0\pi^0$	$\pi^+\pi^-, K^0_S\pi^0$	$\pi^+\pi^-, K^0_S\eta$	$\pi^+\pi^-, K^0_S\omega$	$K^0_S\pi^0\pi^0, K^0_S\pi^0\pi^0$	$K^0_S\pi^0\pi^0, K^0_S\pi^0$	$K^0_S\pi^0\pi^0, K^0_S\eta$	$K^0_S\pi^0\pi^0, K^0_S\omega$	$K^0_S\pi^0, K^0_S\pi^0$	$K^0_S\pi^0, K^0_S\eta$	$K^0_S\pi^0, K^0_S\omega$	$K^0_S\eta, K^0_S\eta$	$K^0_S\eta, K^0_S\omega$	$K^0_S\omega, K^0_S\omega$
$K^-\pi^+$	−0	−0	0	7	3	6	−0	0	6	2	6	0	2	0	3	0	0	1	−0	0	1
$K^+\pi^-$	−0	−0	0	7	3	6	−0	0	6	2	6	0	2	0	3	0	0	1	−0	0	1
K^+K^-	6	2	1	13	5	9	−0	0	3	1	3	0	1	0	2	0	0	1	−0	0	0
$\pi^+\pi^-$	−0	2	0	2	1	2	11	1	8	3	7	0	1	0	2	0	0	0	−0	0	0
$K^0_S\pi^0\pi^0$	−0	−0	1	19	1	11	−0	0	13	1	10	1	42	9	33	2	0	6	−0	0	2
$K^0_S\pi^0$	−0	−0	0	24	2	13	−0	0	16	1	11	0	41	8	31	2	0	7	−0	0	2
$K^0_S\eta$	−0	−0	0	3	15	2	−0	0	2	11	1	0	3	9	3	0	1	1	2	1	0
$K^0_S\omega$	−0	−0	0	17	2	17	−0	0	13	2	14	0	31	6	30	1	0	20	−0	3	9
$K^-\pi^+, K^-\pi^+$	−0	−0	0	0	0	0	−0	0	0	0	0	0	0	0	0	0	0	0	−0	0	0
$K^-\pi^+, K^+\pi^-$	−0	−0	0	5	2	4	−0	0	4	2	4	0	1	0	2	0	0	1	−0	0	0
$K^-\pi^+, K^+K^-$	−0	−0	0	2	1	2	−0	0	1	1	1	0	0	0	1	0	0	0	−0	0	0
$K^-\pi^+, \pi^+\pi^-$	−0	−0	0	1	0	1	−0	0	2	1	2	0	0	0	1	0	0	0	−0	0	0
$K^-\pi^+, K^0_S\pi^0\pi^0$	−0	−0	0	9	1	6	−0	0	7	0	5	0	19	4	15	1	0	3	−0	0	1
$K^-\pi^+, K^0_S\pi^0$	−0	−0	0	9	1	5	−0	0	6	1	5	0	14	3	11	1	0	2	−0	0	1
$K^-\pi^+, K^0_S\eta$	−0	−0	0	1	3	1	−0	0	1	3	1	0	1	2	1	0	0	0	−0	0	0
$K^-\pi^+, K^0_S\omega$	−0	−0	0	7	1	6	−0	0	5	1	5	0	11	2	11	0	0	8	−0	1	3
$K^+\pi^-, K^+\pi^-$	−0	−0	0	0	0	0	−0	0	0	0	0	0	0	0	0	0	0	0	−0	0	0
$K^+\pi^-, K^+K^-$	−0	−0	0	3	1	2	−0	0	1	1	2	0	0	0	1	0	0	0	−0	0	0
$K^+\pi^-, \pi^+\pi^-$	−0	−0	0	1	1	1	−0	0	2	1	2	0	0	0	1	0	0	0	−0	0	0
$K^+\pi^-, K^0_S\pi^0\pi^0$	−0	−0	0	9	1	6	−0	0	7	0	5	0	19	4	15	1	0	3	−0	0	1
$K^+\pi^-, K^0_S\pi^0$	−0	−0	0	9	1	6	−0	0	7	1	5	0	15	3	12	1	0	3	−0	0	1
$K^+\pi^-, K^0_S\eta$	−0	−0	0	1	3	1	−0	0	1	2	1	0	1	2	1	0	0	0	−0	0	0
$K^+\pi^-, K^0_S\omega$	−0	−0	0	7	1	6	−0	0	5	1	5	0	11	2	10	0	0	8	−0	1	3

TABLE XXVIII. Correlation coefficients (%), with statistical and systematic uncertainties, for the efficiency-corrected, background-subtracted yields in Tables XXIV and XXV.

	$X^+e^-\bar{\nu}_e, K^-\pi^+$	$X^+e^-\bar{\nu}_e, K^-K^+$	$X^+e^-\bar{\nu}_e, \pi^-\pi^+$	$X^+e^-\bar{\nu}_e, K^0_S\pi^0\pi^0$	$X^+e^-\bar{\nu}_e, K^0_S\pi^0$	$X^+e^-\bar{\nu}_e, K^0_S\eta$	$X^+e^-\bar{\nu}_e, K^0_S\omega$	$X^-e^+\nu_e, K^+\pi^-$	$X^-e^+\nu_e, K^-K^+$	$X^-e^+\nu_e, \pi^-\pi^+$	$X^-e^+\nu_e, K^0_S\pi^0\pi^0$	$X^-e^+\nu_e, K^0_S\pi^0$	$X^-e^+\nu_e, K^0_S\eta$	$X^-e^+\nu_e, K^0_S\omega$	$K^0_L\pi^0, K^-\pi^+$	$K^0_L\pi^0, K^+\pi^-$	$K^0_L\pi^0, K^+K^-$	$K^0_L\pi^0, \pi^+\pi^-$	$K^0_L\pi^0, K^0_S\pi^0\pi^0$	$K^0_L\pi^0, K^0_S\pi^0$	$K^0_L\pi^0, K^0_S\eta$	$K^0_L\pi^0, K^0_S\omega$
$K^-\pi^+$	43	7	6	1	4	2	6	34	7	8	2	5	2	6	17	15	−0	−0	−0	2	1	5
$K^+\pi^-$	36	7	6	1	4	2	6	43	7	8	2	5	2	6	15	18	−0	−0	−0	2	1	5
K^+K^-	22	28	3	1	3	1	3	22	27	4	1	3	1	3	9	10	0	−0	−0	2	1	3
$\pi^+\pi^-$	14	2	18	1	2	1	3	13	2	17	1	2	1	3	5	6	−0	2	−0	1	0	3
$K^0_S\pi^0\pi^0$	2	0	0	28	26	1	16	2	0	0	34	30	1	16	35	36	−1	−0	0	49	13	36
$K^0_S\pi^0$	3	1	1	16	36	3	18	3	1	1	24	40	2	18	35	36	−2	−1	−1	55	14	38
$K^0_S\eta$	2	0	0	1	3	29	2	2	0	0	2	4	27	2	0	1	−1	−0	−0	3	23	2
$K^0_S\omega$	8	2	2	12	23	3	31	8	2	2	19	27	2	32	29	30	−1	−0	−1	40	11	39
$K^-\pi^+, K^-\pi^+$	0	0	0	0	0	0	0	0	0	0	0	0	0	0	0	0	−0	−0	−0	0	0	0
$K^-\pi^+, K^+\pi^-$	24	5	4	1	3	1	4	23	5	5	1	3	1	4	10	10	−0	−0	−0	1	1	4
$K^-\pi^+, K^+K^-$	8	2	1	0	1	0	1	8	2	2	0	1	0	1	3	4	−0	−0	−0	0	0	1
$K^-\pi^+, \pi^+\pi^-$	7	1	2	0	1	0	1	7	1	3	0	1	0	1	3	3	−0	−0	−0	0	0	1
$K^-\pi^+, K^0_S\pi^0\pi^0$	4	1	1	8	12	1	8	4	1	1	12	14	1	8	17	18	−0	−0	−0	23	6	17
$K^-\pi^+, K^0_S\pi^0$	6	1	1	6	11	1	7	5	1	1	9	12	1	7	8	14	−0	−0	−0	18	5	14
$K^-\pi^+, K^0_S\eta$	2	0	0	0	1	5	1	2	0	1	0	1	5	1	1	1	−0	−0	−0	1	5	1
$K^-\pi^+, K^0_S\omega$	6	1	1	4	8	1	9	6	1	2	7	10	1	9	12	12	−0	−0	−0	14	4	13
$K^+\pi^-, K^+\pi^-$	0	0	0	0	0	0	0	0	0	0	0	0	0	0	0	0	−0	−0	−0	0	0	0
$K^+\pi^-, K^+K^-$	10	3	2	0	1	1	1	9	3	2	0	1	0	1	4	4	−0	−0	−0	1	0	1
$K^+\pi^-, \pi^+\pi^-$	7	1	2	0	1	0	1	7	1	3	0	1	0	1	3	3	−0	−0	−0	0	0	1
$K^+\pi^-, K^0_S\pi^0\pi^0$	4	1	1	8	12	1	8	4	1	1	12	14	1	8	17	18	−0	−0	−0	22	6	17
$K^+\pi^-, K^0_S\pi^0$	6	1	1	6	12	1	8	6	1	1	9	14	1	8	15	10	−0	−0	−0	20	5	15
$K^+\pi^-, K^0_S\eta$	2	0	0	0	1	5	1	2	0	1	0	1	5	1	1	1	−0	−0	−0	1	5	1
$K^+\pi^-, K^0_S\omega$	6	1	1	4	8	1	9	6	1	1	7	9	1	9	11	12	−0	−0	−0	14	4	13

TABLE XXIX. Correlation coefficients (%), with statistical and systematic uncertainties, for the efficiency-corrected, background-subtracted yields in Tables XXIV and XXV. Coefficients of 100% are represented by dots (···).

	K^+K^-, K^+K^-	$K^+K^-, \pi^+\pi^-$	$K^+K^-, K^0_S\pi^0\pi^0$	$K^+K^-, K^0_S\pi^0$	$K^+K^-, K^0_S\eta$	$K^+K^-, K^0_S\omega$	$\pi^+\pi^-, \pi^+\pi^-$	$\pi^+\pi^-, K^0_S\pi^0\pi^0$	$\pi^+\pi^-, K^0_S\pi^0$	$\pi^+\pi^-, K^0_S\eta$	$\pi^+\pi^-, K^0_S\omega$	$K^0_S\pi^0\pi^0, K^0_S\pi^0\pi^0$	$K^0_S\pi^0\pi^0, K^0_S\pi^0$	$K^0_S\pi^0\pi^0, K^0_S\eta$	$K^0_S\pi^0\pi^0, K^0_S\omega$	$K^0_S\pi^0, K^0_S\pi^0$	$K^0_S\pi^0, K^0_S\eta$	$K^0_S\pi^0, K^0_S\omega$	$K^0_S\eta, K^0_S\eta$	$K^0_S\eta, K^0_S\omega$	$K^0_S\omega, K^0_S\omega$
K^+K^-, K^+K^-	···	0	−0	−0	−0	−0	0	−0	−0	−0	−0	−0	−0	−0	−0	−0	−0	−0	−0	0	−0	−0
$K^+K^-, \pi^+\pi^-$		···	−0	−0	−0	−0	0	0	−0	−0	−0	−0	−0	−0	−0	−0	−0	−0	−0	0	−0	−0
$K^+K^-, K^0_S\pi^0\pi^0$			···	0	0	0	−0	0	0	0	0	0	0	0	0	0	0	0	0	−0	0	0
$K^+K^-, K^0_S\pi^0$				···	1	4	−0	0	4	0	3	0	10	2	8	0	0	2	−0	−0	0	1
$K^+K^-, K^0_S\eta$					···	1	−0	0	0	1	0	0	1	1	0	0	0	0	−0	−0	0	0
$K^+K^-, K^0_S\omega$						···	−0	0	2	0	2	0	6	1	5	0	0	2	−0	−0	0	1
$\pi^+\pi^-, \pi^+\pi^-$							···	0	−0	−0	−0	−0	−0	−0	−0	−0	−0	−0	−0	0	−0	−0
$\pi^+\pi^-, K^0_S\pi^0\pi^0$								···	0	0	0	0	0	0	0	0	0	0	−0	0	0	0
$\pi^+\pi^-, K^0_S\pi^0$									···	1	3	0	7	1	5	0	0	1	−0	0	0	0
$\pi^+\pi^-, K^0_S\eta$										···	0	0	0	1	0	0	0	0	−0	0	0	0
$\pi^+\pi^-, K^0_S\omega$											···	0	5	1	4	0	0	2	−0	0	1	0
$K^0_S\pi^0\pi^0, K^0_S\pi^0\pi^0$												···	0	0	0	0	0	0	−0	0	0	0
$K^0_S\pi^0\pi^0, K^0_S\pi^0$													···	4	15	1	0	3	−0	0	1	0
$K^0_S\pi^0\pi^0, K^0_S\eta$														···	3	0	0	1	−0	0	0	0

TABLE XXIX. (*Continued*)

	K^+K^-, K^+K^-	$K^+K^-, \pi^+\pi^-$	$K^+K^-, K^0_S\pi^0\pi^0$	$K^+K^-, K^0_S\pi^0$	$K^+K^-, K^0_S\eta$	$K^+K^-, K^0_S\omega$	$\pi^+\pi^-, \pi^+\pi^-$	$\pi^+\pi^-, K^0_S\pi^0\pi^0$	$\pi^+\pi^-, K^0_S\pi^0$	$\pi^+\pi^-, K^0_S\eta$	$\pi^+\pi^-, K^0_S\omega$	$K^0_S\pi^0\pi^0, K^0_S\pi^0\pi^0$	$K^0_S\pi^0\pi^0, K^0_S\pi^0$	$K^0_S\pi^0\pi^0, K^0_S\eta$	$K^0_S\pi^0\pi^0, K^0_S\omega$	$K^0_S\pi^0, K^0_S\pi^0$	$K^0_S\pi^0, K^0_S\eta$	$K^0_S\pi^0, K^0_S\omega$	$K^0_S\eta, K^0_S\eta$	$K^0_S\eta, K^0_S\omega$	$K^0_S\omega, K^0_S\omega$
$K^0_S\pi^0\pi^0, K^0_S\omega$															⋯	1	0	4	−0	0	2
$K^0_S\pi^0, K^0_S\pi^0$																⋯	0	0	−0	0	0
$K^0_S\pi^0, K^0_S\eta$																	⋯	0	−0	0	0
$K^0_S\pi^0, K^0_S\omega$																		⋯	−0	1	4
$K^0_S\eta, K^0_S\eta$																			⋯	−0	−0
$K^0_S\eta, K^0_S\omega$																				⋯	1
$K^0_S\omega, K^0_S\omega$																					⋯

TABLE XXX. Correlation coefficients (%), with statistical and systematic uncertainties, for the efficiency-corrected, background-subtracted yields in Tables XXIV and XXV.

	$X^+e^-\bar{\nu}_e, K^-\pi^+$	$X^+e^-\bar{\nu}_e, K^-K^+$	$X^+e^-\bar{\nu}_e, \pi^-\pi^+$	$X^+e^-\bar{\nu}_e, K^0_S\pi^0\pi^0$	$X^+e^-\bar{\nu}_e, K^0_S\pi^0$	$X^+e^-\bar{\nu}_e, K^0_S\eta$	$X^+e^-\bar{\nu}_e, K^0_S\omega$	$X^-e^+\nu_e, K^+\pi^-$	$X^-e^+\nu_e, K^-K^+$	$X^-e^+\nu_e, \pi^-\pi^+$	$X^-e^+\nu_e, K^0_S\pi^0\pi^0$	$X^-e^+\nu_e, K^0_S\pi^0$	$X^-e^+\nu_e, K^0_S\eta$	$X^-e^+\nu_e, K^0_S\omega$	$K^0_L\pi^0, K^-\pi^+$	$K^0_L\pi^0, K^+\pi^-$	$K^0_L\pi^0, K^+K^-$	$K^0_L\pi^0, \pi^+\pi^-$	$K^0_L\pi^0, K^0_S\pi^0\pi^0$	$K^0_L\pi^0, K^0_S\pi^0$	$K^0_L\pi^0, K^0_S\eta$	$K^0_L\pi^0, K^0_S\omega$
K^+K^-, K^+K^-	−0	−0	−0	−0	−0	−0	−0	−0	−0	−0	−0	−0	−0	−0	−0	−0	0	0	0	−0	−0	−0
$K^+K^-, \pi^+\pi^-$	−0	−0	−0	−0	−0	−0	−0	−0	−0	−0	−0	−0	−0	−0	−0	−0	0	0	0	−0	−0	−0
$K^+K^-, K^0_S\pi^0\pi^0$	0	0	0	0	0	0	0	0	0	0	0	0	0	0	0	0	−0	−0	−0	0	0	0
$K^+K^-, K^0_S\pi^0$	3	1	0	4	7	1	5	3	1	1	6	8	1	5	9	10	−27	−0	−0	13	3	9
$K^+K^-, K^0_S\eta$	1	0	0	0	1	3	0	1	0	0	0	1	3	0	0	1	−0	−0	−0	1	3	1
$K^+K^-, K^0_S\omega$	3	1	1	2	4	1	4	3	1	1	3	5	0	4	6	6	−0	−0	−0	7	2	6
$\pi^+\pi^-, \pi^+\pi^-$	−0	−0	−0	−0	−0	−0	−0	−0	−0	−0	−0	−0	−0	−0	−0	−0	0	0	0	−0	−0	−0
$\pi^+\pi^-, K^0_S\pi^0\pi^0$	0	0	−0	0	0	0	0	0	0	−0	0	0	0	0	0	0	−0	−0	−0	0	0	0
$\pi^+\pi^-, K^0_S\pi^0$	3	0	1	3	5	1	3	3	0	1	4	6	0	3	7	7	−0	−18	−0	9	2	7
$\pi^+\pi^-, K^0_S\eta$	1	0	0	0	0	2	0	1	0	1	0	1	2	0	0	0	−0	−0	−0	0	2	0
$\pi^+\pi^-, K^0_S\omega$	3	0	1	2	4	0	3	3	0	1	3	4	0	3	5	5	−0	−0	−0	6	2	6
$K^0_S\pi^0\pi^0, K^0_S\pi^0\pi^0$	0	0	0	0	0	0	0	0	0	0	0	0	0	0	0	0	−0	−0	−0	0	0	0
$K^0_S\pi^0\pi^0, K^0_S\pi^0$	1	0	0	8	13	1	8	1	0	0	12	15	1	8	17	17	−0	−0	−21	24	6	17
$K^0_S\pi^0\pi^0, K^0_S\eta$	0	0	0	2	3	2	2	0	0	0	2	3	1	2	3	3	−0	−0	−0	5	3	3
$K^0_S\pi^0\pi^0, K^0_S\omega$	2	0	0	6	10	1	7	2	0	0	9	12	1	8	13	14	−0	−0	−0	19	5	15
$K^0_S\pi^0, K^0_S\pi^0$	0	0	0	0	1	0	0	0	0	0	0	1	0	0	1	1	−0	−0	−0	1	0	1
$K^0_S\pi^0, K^0_S\eta$	0	0	0	0	0	0	0	0	0	0	0	0	0	0	0	0	−0	−0	−0	0	0	0
$K^0_S\pi^0, K^0_S\omega$	0	0	0	1	2	0	5	0	0	0	2	2	0	5	3	3	−0	−0	−0	4	1	5
$K^0_S\eta, K^0_S\eta$	−0	−0	−0	−0	−0	−0	−0	−0	−0	−0	−0	−0	−0	−0	−0	−0	0	0	0	−0	−0	−0
$K^0_S\eta, K^0_S\omega$	0	0	0	0	0	0	1	0	0	0	0	0	0	1	0	0	−0	−0	−0	0	0	1
$K^0_S\omega, K^0_S\omega$	0	0	0	0	1	0	2	0	0	0	1	1	0	2	1	1	−0	−0	−0	1	0	2

TABLE XXXI. Correlation coefficients (%), with statistical and systematic uncertainties, for the efficiency-corrected, background-subtracted yields in Tables XXIV and XXV. Coefficients of 100% are represented by dots ($\cdots$).

	$X^+e^-\bar{\nu}_e, K^-\pi^+$	$X^+e^-\bar{\nu}_e, K^-K^+$	$X^+e^-\bar{\nu}_e, \pi^-\pi^+$	$X^+e^-\bar{\nu}_e, K^0_S\pi^0\pi^0$	$X^+e^-\bar{\nu}_e, K^0_S\pi^0$	$X^+e^-\bar{\nu}_e, K^0_S\eta$	$X^+e^-\bar{\nu}_e, K^0_S\omega$	$X^-e^+\nu_e, K^+\pi^-$	$X^-e^+\nu_e, K^-K^+$	$X^-e^+\nu_e, \pi^-\pi^+$	$X^-e^+\nu_e, K^0_S\pi^0\pi^0$	$X^-e^+\nu_e, K^0_S\pi^0$	$X^-e^+\nu_e, K^0_S\eta$	$X^-e^+\nu_e, K^0_S\omega$	$K^0_L\pi^0, K^-\pi^+$	$K^0_L\pi^0, K^+\pi^-$	$K^0_L\pi^0, K^+K^-$	$K^0_L\pi^0, \pi^+\pi^-$	$K^0_L\pi^0, K^0_S\pi^0\pi^0$	$K^0_L\pi^0, K^0_S\pi^0$	$K^0_L\pi^0, K^0_S\eta$	$K^0_L\pi^0, K^0_S\omega$
$X^+e^-\bar{\nu}_e, K^-\pi^+$	$\cdots$	8	6	3	9	4	7	36	8	8	4	10	4	7	7	7	−0	−0	−0	1	1	3
$X^+e^-\bar{\nu}_e, K^-K^+$		$\cdots$	1	1	2	1	1	8	2	2	1	2	1	1	1	1	−0	−0	−0	0	0	0
$X^+e^-\bar{\nu}_e, \pi^-\pi^+$			$\cdots$	0	2	1	1	6	1	2	1	2	1	1	1	1	−0	−0	−0	0	0	1
$X^+e^-\bar{\nu}_e, K^0_S\pi^0\pi^0$				$\cdots$	6	1	4	3	1	1	5	7	1	4	7	7	−0	−0	−0	10	2	7
$X^+e^-\bar{\nu}_e, K^0_S\pi^0$					$\cdots$	2	7	9	2	2	9	14	2	7	12	12	−0	−0	−0	17	5	12
$X^+e^-\bar{\nu}_e, K^0_S\eta$						$\cdots$	1	4	1	1	1	2	5	1	0	0	−0	−0	−0	1	6	1
$X^+e^-\bar{\nu}_e, K^0_S\omega$							$\cdots$	7	1	2	6	8	1	7	8	8	−0	−0	−0	10	3	9
$X^-e^+\nu_e, K^+\pi^-$								$\cdots$	8	8	4	10	4	7	6	6	−0	−0	−0	1	0	2
$X^-e^+\nu_e, K^-K^+$									$\cdots$	2	1	2	1	1	1	1	−0	−0	−0	0	0	0
$X^-e^+\nu_e, \pi^-\pi^+$										$\cdots$	1	2	1	2	1	1	−0	−0	−0	0	0	1
$X^-e^+\nu_e, K^0_S\pi^0\pi^0$											$\cdots$	10	1	6	11	11	−0	−0	−0	15	4	11
$X^-e^+\nu_e, K^0_S\pi^0$												$\cdots$	2	9	13	14	−0	−0	−0	20	5	14
$X^-e^+\nu_e, K^0_S\eta$													$\cdots$	1	0	0	−0	−0	−0	1	5	1
$X^-e^+\nu_e, K^0_S\omega$														$\cdots$	8	8	−0	−0	−0	10	3	10
$K^0_L\pi^0, K^-\pi^+$															$\cdots$	25	−0	−0	0	26	7	19
$K^0_L\pi^0, K^+\pi^-$																$\cdots$	−0	−0	0	26	7	20
$K^0_L\pi^0, K^+K^-$																	$\cdots$	0	0	−0	−0	−0
$K^0_L\pi^0, \pi^+\pi^-$																		$\cdots$	0	−0	−0	−0
$K^0_L\pi^0, K^0_S\pi^0\pi^0$																			$\cdots$	−0	−0	−0
$K^0_L\pi^0, K^0_S\pi^0$																				$\cdots$	9	24
$K^0_L\pi^0, K^0_S\eta$																					$\cdots$	7
$K^0_L\pi^0, K^0_S\omega$																						$\cdots$

[1] S. L. Glashow, J. Iliopoulos, and L. Maiani, Phys. Rev. D **2**, 1285 (1970).
[2] M. Kobayashi and T. Maskawa, Prog. Theor. Phys. **49**, 652 (1973).
[3] S. Bianco, F. L. Fabbri, D. Benson, and I. Bigi, Riv. Nuovo Cimento Soc. Ital. Fis. **26N7**, 1 (2003).
[4] L. M. Zhang *et al.* (Belle Collaboration), Phys. Rev. Lett. **96**, 151801 (2006).
[5] M. Staric *et al.* (Belle Collaboration), Phys. Rev. Lett. **98**, 211803 (2007).
[6] L. M. Zhang *et al.* (BELLE Collaboration), Phys. Rev. Lett. **99**, 131803 (2007).
[7] B. Aubert *et al.* (*BABAR* Collaboration), Phys. Rev. Lett. **98**, 211802 (2007).
[8] T. Aaltonen *et al.* (CDF Collaboration), Phys. Rev. Lett. **100**, 121802 (2008).
[9] M. Gronau, Y. Grossman, and J. L. Rosner, Phys. Lett. B **508**, 37 (2001).
[10] R. L. Kingsley, S. B. Treiman, F. Wilczek, and A. Zee, Phys. Rev. D **11**, 1919 (1975).
[11] L. B. Okun, B. M. Pontecorvo, and V. I. Zakharov, Lett. Nuovo Cimento Soc. Ital. Fis. **13**, 218 (1975).
[12] R. L. Kingsley, Phys. Lett. B **63**, 329 (1976).
[13] M. Goldhaber and J. L. Rosner, Phys. Rev. D **15**, 1254 (1977).
[14] I. I. Bigi and A. I. Sanda, Phys. Lett. B **171**, 320 (1986).
[15] I. I. Bigi, Report No. SLAC-PUB-4000, Invited talk given at Workshop on Physics Simulation at High Energies, Madison, WI, 5–16, 1986.
[16] I. I. Bigi, Report No. UND-HEP-89-BIG01, also Report No. SLAC-R-343, p. 169, Given at Tau Charm Factory Workshop, Stanford, CA, 23–27, 1989.
[17] Z. Z. Xing, Phys. Rev. D **55**, 196 (1997).
[18] D. Atwood and A. A. Petrov, Phys. Rev. D **71**, 054032 (2005).
[19] D. M. Asner and W. M. Sun, Phys. Rev. D **73**, 034024 (2006); **77**, 019901(E) (2008).
[20] Q. He *et al.* (CLEO Collaboration), Phys. Rev. Lett. **95**, 121801 (2005); **96**, 199903(E) (2006).
[21] W. M. Sun, Nucl. Instrum. Methods Phys. Res., Sect. A **556**, 325 (2006).
[22] Y. Kubota *et al.*, Nucl. Instrum. Methods Phys. Res., Sect. A **320**, 66 (1992).
[23] T. S. Hill, Nucl. Instrum. Methods Phys. Res., Sect. A **418**, 32 (1998).
[24] D. Peterson *et al.*, Nucl. Instrum. Methods Phys. Res., Sect. A **478**, 142 (2002).
[25] M. Artuso *et al.*, Nucl. Instrum. Methods Phys. Res., Sect. A **502**, 91 (2003);

[26] R. A. Briere *et al.* (CLEO-c/CESR-c Taskforces and CLEO-c Collaboration), Cornell LEPP Report No. CLNS 01/1742 (2001).
[27] S. Dobbs *et al.* (CLEO Collaboration), Phys. Rev. D **76**, 112001 (2007).
[28] W.-M. Yao *et al.*, J. Phys. G **33**, 1 (2006).
[29] H. Albrecht *et al.* (ARGUS Collaboration), Phys. Lett. B **241**, 278 (1990).
[30] T. E. Coan *et al.* (CLEO Collaboration), Phys. Rev. Lett. **95**, 181802 (2005).
[31] Q. He *et al.* (CLEO Collaboration), Phys. Rev. Lett. **100**, 091801 (2008).
[32] S. Eidelman *et al.*, Phys. Lett. B **592**, 1 (2004).
[33] E. M. Aitala *et al.* (E791 Collaboration), Phys. Rev. D **57**, 13 (1998).
[34] J. M. Link *et al.* (FOCUS Collaboration), Phys. Lett. B **618**, 23 (2005).
[35] A. Abulencia *et al.* (CDF Collaboration), Phys. Rev. D **74**, 031109 (2006).
[36] E. M. Aitala *et al.* (E791 Collaboration), Phys. Rev. Lett. **77**, 2384 (1996).
[37] C. Cawlfield *et al.* (CLEO Collaboration), Phys. Rev. D **71**, 077101 (2005).
[38] K. Abe *et al.* (Belle Collaboration), Phys. Rev. D **72**, 071101 (2005).
[39] B. Aubert *et al.* (*BABAR* Collaboration), Phys. Rev. D **76**, 014018 (2007).
[40] S. E. Csorna *et al.* (CLEO Collaboration), Phys. Rev. D **65**, 092001 (2002).
[41] E. M. Aitala *et al.* (E791 Collaboration), Phys. Rev. Lett. **83**, 32 (1999).
[42] J. M. Link *et al.* (FOCUS Collaboration), Phys. Lett. B **485**, 62 (2000).
[43] B. Aubert *et al.* (*BABAR* Collaboration), Phys. Rev. Lett. **91**, 121801 (2003).
[44] K. Abe *et al.* (Belle Collaboration), Phys. Rev. Lett. **88**, 162001 (2002).
[45] M. Staric *et al.* (Belle Collaboration), Phys. Rev. Lett. **98**, 211803 (2007).
[46] D. M. Asner *et al.* (CLEO Collaboration), Phys. Rev. D **72**, 012001 (2005).
[47] R. Godang *et al.* (CLEO Collaboration), Phys. Rev. Lett. **84**, 5038 (2000).
[48] E. M. Aitala *et al.* (E791 Collaboration), Phys. Lett. B **421**, 405 (1998).
[49] J. M. Link *et al.* (FOCUS Collaboration), Phys. Lett. B **555**, 167 (2003).
[50] D. Acosta *et al.* (CDF Collaboration), Phys. Rev. Lett. **94**, 122001 (2005).
[51] P. Rubin *et al.* (CLEO Collaboration), Phys. Rev. Lett. **96**, 081802 (2006).
[52] J. Alexander *et al.* (CLEO Collaboration), Phys. Rev. Lett. **100**, 161804 (2008).
[53] E. Barberio and Z. Was, Comput. Phys. Commun. **79**, 291 (1994).
[54] A. Petrov (private communication).